

Document downloaded from:

<http://hdl.handle.net/10251/47799>

This paper must be cited as:

Gomis, O.; Vilaplana, R.; Manjon, F. J.; et ál.. (2011). Lattice dynamics of Sb₂Te₃ at high pressures. *Physical Review B*. 84:174305-1-174305-12.
doi:10.1103/PhysRevB.84.174305.



The final publication is available at

<http://journals.aps.org/prb/pdf/10.1103/PhysRevB.84.174305>

Copyright American Physical Society

Study of the lattice dynamics of Sb_2Te_3 at high pressures

O. Gomis,^{1,*} R. Vilaplana,¹ F.J. Manjón,² P. Rodríguez-Hernández,³
E. Pérez-González,³ A. Muñoz,³ V. Kucek⁴, and C. Drasar⁴

¹Centro de Tecnologías Físicas, MALTA Consolider Team, Universitat Politècnica de València, 46022 Valencia (Spain)

²Instituto de Diseño para la Fabricación y Producción Automatizada, MALTA Consolider Team, Universitat Politècnica de València, 46022 Valencia (Spain)

³MALTA Consolider Team - Departamento de Física Fundamental II, and Instituto U. de Materiales y Nanotecnología, Universidad de La Laguna, Universidad de La Laguna, 38205 La Laguna, Tenerife (Spain)

⁴Faculty of Chemical Technology, University of Pardubice, Studentská 95, 53210-Pardubice, (Czech Republic)

Abstract. We report an experimental and theoretical lattice dynamics study of antimony telluride (Sb_2Te_3) up to 26 GPa together with a theoretical study of its structural stability under pressure. Raman-active modes of the low-pressure rhombohedral (R-3m) phase were observed up to 7.7 GPa. Changes of the frequencies and linewidths were observed around 3.5 GPa where an electronic topological transition was previously found. Raman mode changes evidence phase transitions at 7.7, 14.5, and 25 GPa. The frequencies and pressure coefficients of the new phases above 7.7 and 14.5 GPa agree with those calculated for the monoclinic C2/m and C2/c structures recently observed at high pressures in Bi_2Te_3 , and also for the C2/m phase in the case of Bi_2Se_3 and Sb_2Te_3 . Above 25 GPa no Raman-active modes are observed in Sb_2Te_3 similarly to the case of Bi_2Te_3 and Bi_2Se_3 . Therefore, it is possible that the structure of Sb_2Te_3 above 25 GPa is the same disordered bcc phase already found in Bi_2Te_3 by x-ray diffraction studies. Upon pressure release, Sb_2Te_3 reverts back to the original rhombohedral phase after considerable hysteresis. Raman- and IR-mode symmetries, frequencies and pressure coefficients in the different phases are reported and discussed.

Key words: high pressure, topological insulators, thermoelectric materials, Raman scattering, *ab initio* calculations

PACS: 62.50.-p,63.20.-e,64.70.K-,61.50.Ks

I. Introduction

Antimony telluride (Sb_2Te_3) is a layered chalcogenide with great interest for applications in thermoelectric devices [1]. The thermoelectric properties of Sb_2Te_3 and their alloys have been extensively studied due to their promising operation in the temperature range of 300-500 K [2,3], and an enhancement of the thermoelectric properties has been recently found by nanostructuring these semiconductors due to the occurrence of quantum size effect and increased interface scattering of phonons [4,5]. Furthermore, in the last years Sb_2Te_3 has been proposed as a candidate to substitute flash memories by phase-change memories (PRAM) due to the excellent properties of Sb_2Te_3 and related materials, like excellent endurance, non-destructive reading, direct overwriting, low-programming energy, huge-read dynamic range, fast speed, high performance, multistate storage, and good complementary metal-oxide-semiconductor logic compatibility [6,7].

Sb_2Te_3 is a narrow bandgap semiconductor with tetradymite crystal structure [R-3m, space group (S.G.) 166, Z=3] [8]. This rhombohedral layered structure is formed by 5 hexagonal close packed atomic sublayers (Te-Sb-Te-Sb-Te) linked by van der Waals forces and it is common to other narrow bandgap semiconductor chalcogenides, like Bi_2Te_3 and Bi_2Se_3 . Studies of these three materials are an actual hot topic because they were recently predicted to behave as topological insulators [9]; i.e., a new class of materials that behave as insulators in the bulk but conduct electric current in the surface. These topological insulators are characterized by the presence of a strong spin-orbit coupling that leads to the opening of a narrow bandgap and causes certain topological invariants in the bulk to differ from their values in vacuum. The sudden change of invariants at the interface results in metallic, time reversal invariant surface states whose properties are useful for applications in spintronics and quantum computation [10,11]. Therefore, in the recent years a number of papers have been devoted to the search of the 3D topological insulators among Sb_2Te_3 , Bi_2Te_3 , Bi_2Se_3 , and their mixtures, and

* Corresponding author. E-mail address: osgohi@fis.upv.es
Tel.: + 34 96 652 84 26, Fax: + 34 96 652 84 85

different works observed the features of the topological nature of the band structure in the three pure compounds [12-15].

High-pressure studies are very useful to understand materials properties and design new materials because the increase in pressure allows to reduce the interatomic distances and to finely tune the materials properties. It has been verified that the thermoelectric properties of semiconductor chalcogenides improve with increasing pressure and that the study of the properties of these materials could help in the design of better thermoelectric materials by substituting external pressure by chemical pressure [16-20]. Therefore, the electrical and thermoelectric properties of Sb_2Te_3 , Bi_2Te_3 , and Bi_2Se_3 , as well as their electronic band structure, have been studied at high pressures [21-28]. Recent high-pressure studies in these compounds have shown a pressure-induced superconductivity [29,30] that has further stimulated high-pressure studies.

In particular, structural studies under pressure in layered chalcogenides Sb_2Te_3 , Bi_2Te_3 , and Bi_2Se_3 are scarce and the determination of the crystalline structures of these materials at high pressures has been a long puzzle [17,24,31,32]. Only recently, the space groups of the high-pressure phases of Bi_2Te_3 have been elucidated by x-ray diffraction (XRD) measurements in a synchrotron facility for phase IV [33] and with the additional help of a particle swarm optimization algorithm for phases II, III and IV [34]. Furthermore, recent high-pressure powder XRD measurements have evidenced a pressure-induced electronic topological transition (ETT) in Bi_2Te_3 around 3.2 GPa as a change in compressibility [30,31,32,35,36,37]. The same ETT has been observed in Bi_2Se_3 around 5 GPa [38] and Sb_2Te_3 around 3.5 GPa [24,31,39]. An ETT or Lifshitz transition occurs when an extreme of the electronic band structure, which is associated to a Van Hove singularity in the density of states, crosses the Fermi energy level [40]. This crossing, which can be driven by pressure, temperature, doping, etc., results in a change in the topology of the Fermi surface that changes the electronic density of states near the Fermi energy. An ETT is a 2.5 transition in the Ehrenfest description of the phase transitions so no discontinuity of the volume (first derivative of the Gibbs free energy) but a change in the compressibility (second derivative of the Gibbs free energy) is expected in the vicinity of the ETT.

The lattice dynamics properties of Sb_2Te_3 have been studied both experimentally and theoretically at room pressure [41,42]. Only the pressure dependence of the lattice dynamics has been studied in $\text{Sb}_{1.5}\text{Bi}_{0.5}\text{Te}_3$ single crystals till 3 GPa [17] and in Sb_2Te_3 nanocrystals till 25 GPa [39]. Since anomalies in the phonon spectrum are also expected

for materials undergoing an ETT [43,44] and have been observed in a number of materials [45-47] as well as in $\text{Sb}_{1.5}\text{Bi}_{0.5}\text{Te}_3$ [31], Bi_2Te_3 [48], and Bi_2Se_3 [38], we want to study the effect of the ETT recently observed in Sb_2Te_3 [24,31,39] by means of Raman scattering measurements. In this work, we report room temperature Raman scattering measurements in Sb_2Te_3 up to 26 GPa together with total-energy and lattice-dynamical *ab initio* calculations as a part of our systematic study of the structural stability and the vibrational properties of the thermoelectric chalcogenide family formed by Bi_2Te_3 , Bi_2Se_3 , and Sb_2Te_3 . We provide evidence that the phase transitions occurring in Sb_2Te_3 seem to be the same observed in the other two members of the family up to 30 GPa. Furthermore, we observe Raman-mode anomalies near 3.5 GPa and a change of tendency in the c/a ratio vs. pressure plot at about 3 GPa from *ab initio* calculations which support the recent observation of a pressure-induced electronic topological transition (ETT) in the rhombohedral phase of Sb_2Te_3 [24,31,39], as predicted by Larson [49].

II. Experimental details

We have used p-type Sb_2Te_3 single crystals that were prepared from stoichiometric mixture of 5N purity elements using the modified Bridgman technique. The detailed description of crystal growth was published elsewhere [50]. Preliminary room temperature measurements on single crystalline samples (15mm x 4mm x 0.3mm) yield in-plane electrical resistivity $\rho_{\perp c} = 2.1 \cdot 10^{-6} \Omega \cdot \text{m}$ and Hall coefficient $R_H(\mathbf{B} \parallel \mathbf{c}) = 0.063 \text{ cm}^3 \text{C}^{-1}$. The latter gives a hole concentration of $7.3 \cdot 10^{19} \text{ cm}^{-3}$ providing the approximation presented in [51]. A sample (100 μm x 100 μm x 5 μm) was inserted in a membrane-type diamond anvil cell (DAC) with a 4:1 methanol-ethanol mixture as pressure-transmitting medium, ensuring hydrostatic conditions up to 10 GPa and quasi-hydrostatic conditions between 10 and 25 GPa [52,53]. Pressure was determined by the ruby luminescence method [54].

Unpolarized room-temperature Raman scattering experiments at high pressures in backscattering geometry were performed using a HeNe laser (6328 Å line) with a power below 5 mW in order not to burn the sample and the signal was collected by a Horiba Jobin Yvon LabRAM HR microspectrometer equipped with a TE-cooled multi-channel CCD detector and with a spectral resolution of 1.5 cm^{-1} . Raman modes in the different phases of Sb_2Te_3 have been modeled by Voigt profiles (Lorentzian profile

convoluted by a Gaussian profile whose linewidth is fixed by to the spectral resolution of the system) so that deconvoluted Lorentzian linewidths have been obtained.

III. *Ab initio* calculations

Two recent works have reported the structures of the high-pressure phases of Bi_2Te_3 up to 25 GPa [33,34]. The ambient pressure phase of Bi_2Te_3 has a rhombohedral ($\alpha\text{-Bi}_2\text{Te}_3$) structure and the second ($\beta\text{-Bi}_2\text{Te}_3$), and third ($\gamma\text{-Bi}_2\text{Te}_3$) have $C2/m$ (S.G. 12, $Z=4$) and $C2/c$ (S.G. 15, $Z=4$) structures, respectively [34]. As regards the fourth phase ($\delta\text{-Bi}_2\text{Te}_3$), which appears above 14.5 GPa, a disordered bcc phase ($\text{Im-}3m$, S.G. 229, $Z=1$) in which both Bi and Te occupy the same Wyckoff site has been proposed [33,34]. In two recent papers we have studied both experimentally and theoretically the lattice dynamics of Bi_2Te_3 and Bi_2Se_3 at high pressures where we have shown that both compounds seem to undergo the same structural phase transitions [38,48]. In this work we explore the relative stability of these phases in Sb_2Te_3 . We have performed total-energy calculations within the density functional theory (DFT) [55] using the plane-wave method and the pseudopotential theory with the Viena ab initio simulation package (VASP) [56]. We have used the projector-augmented wave scheme (PAW) [57] implemented in this package. Basis set including plane waves up to an energy cutoff of 240 eV were used in order to achieve highly converged results and accurate description of the electronic properties. We have used the generalized gradient approximation (GGA) for the description of the exchange-correlation energy with the PBEsol prescription [58]. Dense special k-points sampling for the Brillouin zone integration were performed in order to obtain very well converged energies and forces. We also use an accurate prescription during the calculations in order to obtain very well converged forces during the calculation of the dynamical matrix. At each selected volume, the structures were fully relaxed to their equilibrium configuration through the calculation of the forces on atoms and the stress tensor. In the relaxed equilibrium configuration, the forces on the atoms are less than 0.002 eV/\AA and the deviation of the stress tensor from a diagonal hydrostatic form is less than 1 kbar (0.1 GPa). The application of DFT-based total-energy calculations to the study of semiconductors properties under high pressure has been reviewed in Ref. 59, showing that the phase stability, electronic and dynamical properties of compounds under pressure are well describe by DFT.

Since the calculation of the disordered bcc phase is not possible to do it with the VASP code we have attempted to perform calculations for the bcc-like monoclinic C2/m structure proposed in Ref. 34. Furthermore, since the thermodynamic phase transition between two structures occurs when the Gibbs free energy (G) is the same for both phases, we have obtained the Gibbs free energy of the different phases using a quasi-harmonic Debye model [60] that allows obtaining G at room temperature from calculations performed for T= 0 K in order to discuss about the relative stability of the different phases proposed in the present work.

In order to fully confirm whether the experimentally measured Raman scattering of the high-pressure phases of Sb₂Te₃ agree with theoretical estimates for these phases, we have also performed lattice dynamics calculations of the phonon modes in the R-3m, C2/m, and C2/c phases at the zone center (Γ point) of the BZ. Our theoretical results enable us to assign the Raman modes observed for the different phases of Sb₂Te₃. Furthermore, the calculations provide information about the symmetry of the modes and polarization vectors which is not readily accessible in the present experiment. Highly converged results on forces are required for the calculation of the dynamical matrix. We use the direct force constant approach (or supercell method) [61]. The construction of the dynamical matrix at the Γ point of the BZ is particularly simple and involves separate calculations of the forces in which a fixed displacement from the equilibrium configuration of the atoms within the *primitive* unit cell is considered. Symmetry aids by reducing the number of such independent displacements, reducing the computational effort in the study of the analyzed structures considered in this work. Diagonalization of the dynamical matrix provides both the frequencies of the normal modes and their polarization vectors. It allows to us to identify the irreducible representation and the character of the phonons modes at the Γ point. In this work we provide and discuss the calculated frequencies and pressure coefficients of the Raman-active modes for the three calculated phases of Sb₂Te₃. The theoretical results obtained for infrared-active modes for the three calculated phases of Sb₂Te₃ are given as supplementary material of this article [62].

Finally, we want to mention that we have also checked the effect of the spin-orbit (SO) coupling in the structural stability and the phonon frequencies of the R-3m phase. We have found that the effect of the SO coupling is very small and do not affect our present results (total energies are quite similar and there are only small differences of 1-3 cm⁻¹ in the phonon frequencies at the Γ point), but increased substantially the

computer time so that the cost of the computation was very high for the more complex monoclinic high-pressure phases, as already discussed in Ref. **34**. Therefore, all the theoretical values discussed in the present paper do not include the SO coupling. In order to test our calculations we show in **Table I** the comparison between the experimental and calculated lattice parameters in the R-3m phase of Sb_2Te_3 at room pressure. As far as the R-3m phase is concerned, our calculations with GGA-PBEsol give results for the lattice parameters that on average are closer to the measured ones than those obtained by the other authors (see **Table I**). In general, GGA-PBEsol gives intermediate results between those obtained by GGA-PBE and by local density approximation (LDA). Calculations with LDA usually underestimate the lattice parameters and the volume with respect to the experimental values while calculations with GGA-PBE tend to overestimate the lattice parameters. Additionally, we give in **Table I** the calculated lattice parameters of Sb_2Te_3 in the C2/m and C2/c structures at 8.6 and 15.2 GPa, respectively, for future comparison with experimental data of x-ray diffraction. Note that in **Table I** the c lattice parameter and β angle for monoclinic C2/m and C2/c structures differ from those obtained by Zhu et al. [**34**]. The reason is that the results of our *ab initio* calculations are given in the standard setting for the monoclinic structures, in contrast with Ref. **34**, for a better comparison to future experiments.

IV. Results and discussion

A. Raman scattering of $\alpha\text{-Sb}_2\text{Te}_3$

The rhombohedral (R-3m) phase of Sb_2Te_3 is a centrosymmetric structure where one Te atom is located in a 3a Wyckoff site and the remaining Sb and Te atoms occupying the 6c Wyckoff sites. Therefore, group theory allows us to predict 10 zone-center modes which decompose in the irreducible representations as follows [**63**]

$$\Gamma_{10} = 2A_{1g} + 3A_{2u} + 2E_g + 3E_u. \quad (1)$$

The two acoustic branches come from one A_{2u} mode and a doubly degenerated E_u mode, while the rest correspond to optic modes. Gerade (g) modes are Raman active while ungerade (u) modes are infrared (IR) active. Therefore, there are four Raman-active modes ($2A_{1g} + 2E_g$) and four IR-active modes ($2A_{2u} + 2E_u$). The E_g modes correspond to atomic vibrations in the plane of the layers, while the A_{1g} modes correspond to vibrations along the c axis perpendicular to the layers [**41,42**].

Figure 1 shows the experimental Raman spectra of rhombohedral Sb_2Te_3 at different pressures up to 7.7 GPa. We have observed and followed under pressure 3 out of the 4 Raman-active modes, and the measured values at room pressure are in good agreement with those reported in the literature [41]. In fact, the E_g mode calculated to be close to 40 cm^{-1} (see **Table II**) has not been observed in our experiments as it was also not seen in previous Raman scattering measurements at room pressure [41]. **Table II** summarizes the experimental and theoretical first-order Raman mode frequencies and pressure coefficients in the rhombohedral phase. As regards the theoretical frequencies for the Raman modes at room pressure, our values using PBEsol are higher than those obtained by Sosso et al. [42] by using GGA-PBE. This result was expected because GGA-PBE calculations usually tend to underestimate phonon frequencies because of the overestimation of lattice parameters. In general, our theoretical and experimental frequencies at ambient pressure for the Raman-active modes in the $\alpha\text{-Sb}_2\text{Te}_3$ show a good agreement with the theoretical values of Sosso et al. [42].

Figure 2(a) shows the experimental pressure dependence of the frequencies of the 3 first-order Raman modes measured in $\alpha\text{-Sb}_2\text{Te}_3$. All Raman modes show an increase in frequency with increasing pressure in good agreement with our theoretical calculations for the Raman-active modes of the R-3m phase. This result contrasts with the decrease in frequency observed for the lowest-frequency mode of A_{1g} symmetry in $\text{Sb}_{1.5}\text{Bi}_{0.5}\text{Te}_3$ [17]. The symmetry of the soft mode in $\text{Sb}_{1.5}\text{Bi}_{0.5}\text{Te}_3$ would be more consistent with the high-frequency E_g mode if we compare its frequency with our measurements and calculations. In **Fig. 2(a)** it can be observed that all measured Raman modes exhibit a hardening with increasing pressure in good agreement with theoretical calculations (see **Table II**); however, a considerable decrease of the pressure coefficient of the three measured Raman modes above 3.5 GPa can be noted [see dashed lines in **Fig. 2 (a)**]. In **Table II** we provide the experimental pressure coefficients at room pressure and at 4.0 GPa in the rhombohedral phase, which can be compared to the theoretical values at room pressure.

A decrease of the pressure coefficients of the Raman-active mode frequencies was previously observed in Bi_2Te_3 and Bi_2Se_3 [38,48]. Since an ETT occurs in these materials at low pressures, we have attributed the less positive pressure coefficient of these three Raman modes above 3.5 GPa to the pressure-induced electronic topological transition (ETT) recently observed in Sb_2Te_3 and Bi_2Te_3 above 3 GPa [31,37,48] and in Bi_2Se_3 around 5 GPa [38]. Furthermore, the anomalies measured in Sb_2Te_3 around 3.5

GPa are consistent with those observed previously in $\text{Sb}_{1.5}\text{Bi}_{0.5}\text{Te}_3$ [17]. In the latter work, the high-frequency A_{1g} mode was not altered near the ETT in good agreement with our measurements; however, we have measured a change both in the lower A_{1g} and the higher-frequency E_g modes. Since A_{1g} modes are polarized in the direction perpendicular to the layers while the E_g modes are polarized along the layers, our observation of a softening of both modes in Sb_2Te_3 suggests that the ETT in Sb_2Te_3 is related to a change of the structural compressibility of both the direction perpendicular to the layers and the direction along the layers. This seems to be different to the case of Bi_2Te_3 since Polian *et al.* suggest that the ETT in Bi_2Te_3 only affects the plane of the layers [37]. Since a similar behavior of the phonon modes near the ETT was observed in Bi_2Te_3 [48] and Bi_2Se_3 [38] more research in this respect is necessary in order to understand the structural and vibrational relationships near the ETT in this family of semiconductors.

In order to check if there are other Raman anomalies that evidence the ETT in Sb_2Te_3 we have also plotted in **Fig. 2(b)** the pressure dependence of the linewidth of the Raman modes of the R-3m phase up to 7.7 GPa. The FWHMs of all modes decrease with pressure up to about 3.5 GPa and show a different behavior above this pressure. Therefore, both our results on the pressure dependence of the frequency and linewidth support to the observation of the ETT around 3.5 GPa in $\alpha\text{-Sb}_2\text{Te}_3$ [31]. At present we have no definite explanation for the sudden change of the pressure coefficient of the linewidth of the three Raman-active modes at 3.5 GPa in this family of compounds, but it is clear that must be related to the ETT since the same behavior has been previously observed in Bi_2Te_3 [48] and Bi_2Se_3 [38].

It is known that pressure shows no net effect in the phonon linewidths of first-order Raman modes [64]. However, an experimental slight increase of the phonon linewidths is usually observed. In this sense, the behavior of the Raman-active modes of Sb_2Te_3 with pressure seems to be normal above 3.5 GPa and anomalous below this pressure. There can be several explanations for the anomalous behavior of the linewidths below 3.5 GPa. In conventional semiconductors it has been observed that the large linewidth is usually caused by a strong phonon-phonon interaction (i.e. anharmonic decay) causing a decrease of the phonon lifetime and therefore an increase in the linewidth. This mechanism is usually related to the coincidence of the first-order Raman-mode frequencies with a high density of the two-phonon (sum) density of states, which in special cases lead to Fermi resonances [64]. In this respect, the decrease of the

linewidth of the Raman-active modes in α -Sb₂Te₃ with increasing pressure up to 3.5 GPa could be understood by the separation of the first-order Raman-active modes with respect to the frequency of the high density of the two-phonon (sum) density of states due to the larger pressure coefficient of the first-order Raman modes than the sum of two-phonon states which usually involves acoustic modes with very small or even negative pressure coefficients. Whether this mechanism is responsible for the decrease of the linewidth of the Raman active modes in α -Sb₂Te₃ and the other members of this family (α -Bi₂Se₃ and α -Bi₂Te₃) is difficult to say but seems not likely because the same effect is observed in almost all Raman-active modes, thus pointing to some electron-phonon coupling perhaps related to the small bandgap energy, which is a common feature of these three materials.

We want to make a comment on the pressure coefficients of the different Raman modes in α -Sb₂Te₃. In chalcogenide laminar materials, the two lowest-frequency E and A modes are usually related to shear vibrations between adjacent layers along the a-b plane and to vibrations of one layer against the others along the c axis, respectively. Usually, the E mode displays the smallest pressure coefficient due to the weak bending force constant between the interlayer bonds (in our case, Te-Te bonds) while the A mode displays the largest pressure coefficient due to the extraordinary increase of the stretching force constant between the interlayer bonds. For example, the E and A modes with frequencies around 40 (60) cm⁻¹ and 116 (133) cm⁻¹ in InSe (GaSe), respectively, have pressure coefficients of 0.68 (0.85) cm⁻¹/GPa and 5.41 (5.78) cm⁻¹/GPa [65,66]. In α -Sb₂Te₃ our theoretical calculations show that the two lowest-frequency A_{1g} and E_g modes have rather similar pressure coefficients thus suggesting that in this compound both interlayer and intralayer bonds increase in force in a similar way with increasing pressure. This is consistent with the weak anisotropy of their properties unlike other layered chalcogenides showing a considerable anisotropy and a much larger difference between their A and E pressure coefficients. We think that the rather strong interlayer bonds in α -Sb₂Te₃ as compared to other layered chalcogenides, like InSe and GaSe, can be due to the strong interlayer interaction occurring in the former favored by the SO coupling which is absent in the other layered chalcogenides. The strong interlayer interaction favored by the SO coupling has been already pointed out in a recent work where it is stressed the importance of considering the SO coupling in theoretical calculations to give account for the correct modeling of the properties of bulk and nanomaterials of these layered chalcogenides with heavy elements like Bi or Sb [67].

Note, however, that our lattice dynamics calculations without SO coupling reproduce well both the frequencies and pressure coefficients of the Raman-active modes in α -Sb₂Te₃ (see comments in section III) and this suggests that the effect of SO coupling in the lattice dynamical properties of this material can be reasonably neglected in our calculations. We think that the reason for the good lattice dynamics results of our calculations, despite not including the SO coupling, is due to the cancellation of two errors. It is well known that *ab initio* calculations do not simulate well van der Waals interactions, like those of interlayer bonds in these layered materials. In fact, these soft interactions are simulated as slightly stronger (ionic-covalent) bonds by *ab initio* calculations. Since the SO coupling leads to hardening of the soft van der Waals interactions, the artificial hardening of the van der Waals interlayer bonds in *ab initio* calculations compensate the lack of the SO coupling in our calculations. This explains why it is not necessary to take into account the SO coupling in the calculations in order to give good account for the lattice dynamics properties in Sb₂Te₃.

Finally, we want to comment that our theoretical calculations provide evidence of the presence of the ETT in Sb₂Te₃ as observed experimentally by our sudden change in the frequency slope of the E_g² mode and the change of the slopes of all the Raman linewidths, and by previous XRD measurements [24,31,39]. **Fig 3** shows in panel (a) the pressure dependence of the *a* and *c* lattice parameters vs. pressure for α -Sb₂Te₃ obtained from our *ab initio* calculations and those from XRD measurements [24,39]. The inset of **Figure 3** shows that the *c/a* ratio vs. pressure dependence for our theoretical and previous experimental data [24,39]. As observed, a good agreement is found between our calculated pressure dependence of the lattice parameters and *c/a* ratio and previous experimental data. It can be observed that both experimental and theoretical *c/a* ratios vs. pressure exhibit a minimum at about 2.5-3.5 GPa indicating a change of behavior in the *c/a* ratio before and after the minimum. The same behavior of *c/a* vs. pressure was already found in Bi₂Te₃ [32,37] and Bi₂Se₃ [38] and was attributed to the presence of the ETT due to a change in the compressibility at the ETT vicinity. Therefore the *c/a* vs. pressure behavior further supports the ETT occurrence in α -Sb₂Te₃ at about 3 GPa. Fig. 3(b) shows the pressure dependence of the unit cell volume from our *ab initio* calculations, and those of XRD measurements [24,31,39]. It can be seen that in general there is a nice agreement between measurements and theoretical values. We have fitted our *ab initio* data to a Birch-Murnaghan equation of state (EOS) obtaining the following results: $V_0 = 474.4 \text{ \AA}^3$, $B_0 = 41.0 \text{ GPa}$, $B_0' = 5.2$. Jacobsen *et al.* reported values of $V_0 =$

479.03(64) Å³, $B_0 = 30.2(14)$ GPa, $B_0' = 9.4(11)$ [31]. We have fitted Sakai *et al.* $V=V(P)$ data [24] with a Birch-Murnaghan EOS obtaining values of $V_0 = 475(3)$ Å³ and $B_0 = 40(4)$ GPa with B_0' fixed to 4. In all the cases the values for V_0 and B_0 are similar and all are summarized in **Table I**.

B. Raman scattering of β -Sb₂Te₃

Reported XRD measurements showed that α -Sb₂Te₃ undergoes a phase transition around 7.5 GPa towards an still unknown phase β -Sb₂Te₃ [24,31]. In fact, a very recent unpublished work reporting XRD and Raman measurements under high pressure in nanocrystalline Sb₂Te₃ demonstrates that the XRD pattern of the β -Sb₂Te₃ is isostructural to that of β -Bi₂Te₃ (the first high-pressure phase of Bi₂Te₃ with C2/m structure) [39]. Additionally, it is worth to mention that a phase of Sb₂Te₃ with C2/m structure which is isostructural to α -As₂Te₃ has been recently found at ambient conditions as a metastable phase after a high-pressure and high-temperature treatment of α -Sb₂Te₃ [68].

In order to obtain information about β -Sb₂Te₃ we show in **Figure 4(a)** the experimental Raman spectra of β -Sb₂Te₃ at different pressures from 8.6 GPa up to 14.5 GPa. Recently, it has been demonstrated that the first high-pressure phase of Bi₂Te₃ (β -Bi₂Te₃) has a monoclinic C2/m structure where all the five Bi and Te atoms occupy 4i Wyckoff sites [34]. Group theoretical considerations predict 30 vibrational modes for the C2/m phase of Sb₂Te₃ with the following representation [63]

$$\Gamma_{30} = (10A_g + 10B_u) + (5B_g + 5A_u). \quad (2)$$

From them, one A_u and two B_u are the acoustic phonons and the rest are optical phonons. Consequently, we expect 15 zone-center Raman-active ($10A_g + 5B_g$) modes for the C2/m phase. For the sake of comparison we have marked the calculated Raman mode frequencies for this phase at 8.6 GPa and have compared it with the Raman spectra at 8.6 GPa in **Fig. 4(a)**. The fit of the Raman spectrum at 8.6 GPa to Voigt profiles can be observed in Fig.1 of the supplementary material [62]. **Figure 4(b)** shows the pressure dependence of the experimental and theoretical first-order Raman mode frequencies in β -Sb₂Te₃. It can be observed that the frequencies of the experimental Raman modes agree reasonably well with our calculations especially for the more

defined peaks above 120 cm^{-1} . Therefore, our Raman measurements confirm that the β - Sb_2Te_3 phase has the monoclinic $C2/m$ structure already found by means of XRD measurements in Bi_2Te_3 [34], Bi_2Se_3 [38], and in Sb_2Te_3 [39]. **Table III** summarizes the experimental and theoretical first-order Raman mode frequencies and pressure coefficients at 8.6 GPa in the β - Sb_2Te_3 phase. In our experiments we have not observed the two lowest-frequency modes B_g^1 and A_g^1 . Their detection is difficult because they can be weak modes and their frequency is below the cutting edge of the Raman edge filter of our LabRAM spectrometer. In the low frequency region, the A_g^2 mode is detected at pressures above 10 GPa as a shoulder of the B_g^2 mode. *Ab initio* calculations show that the B_g^2 and A_g^2 modes are almost degenerate in frequency and with similar pressure coefficients. In the experiment, these two modes have similar pressure coefficients and a small difference in frequency. In the region about $117\text{-}122 \text{ cm}^{-1}$ at 8.6 GPa four modes are theoretically predicted to occur with similar pressure coefficients (see **Fig. 4(b)** and **Table III**). We have been able to follow the B_g^4 and A_g^6 modes separately. The weak band between the B_g^4 and A_g^6 modes has been assigned jointly to B_g^5 and A_g^5 modes. The increase in intensity with pressure of this weak band has helped in its identification. Note that in this experiment the $110\text{-}130 \text{ cm}^{-1}$ range shows several broad and overlapped bands in a short region of frequency that complicates the analysis and assignment of modes due to the proximity of the peaks. In fact, the 15 Raman-active modes in β - Sb_2Te_3 are concentrated in the frequency region between 20 and 200 cm^{-1} .

We want to make a comment on the Sb coordination of β - Sb_2Te_3 . In this respect, at the $R\text{-}3m$ to $C2/m$ phase transition pressure, the highest-frequency mode of β - Sb_2Te_3 has a smaller frequency (172 cm^{-1}) than the highest-frequency mode of α - Sb_2Te_3 (185 cm^{-1}). This decrease in frequency of the highest-frequency mode, usually related to stretching Sb-Te vibrations, suggests an increase in the Sb-Te distance related to an increase of the Sb coordination from sixfold in α - Sb_2Te_3 to sevenfold in β - Sb_2Te_3 . This result is in good agreement with the recently observed increase of the Bi coordination on going from the rhombohedral to the $C2/m$ structures in Bi_2Te_3 [34,48] Bi_2Se_3 [38], and Sb_2Te_3 [39].

Finally, we want to mention that it is curious that our Raman experiments for the β - Sb_2Te_3 show quite a lot of the Raman modes theoretically predicted for that phase. However, in the work of Ref. 39 the authors find for the β - Sb_2Te_3 much less Raman modes than those theoretically predicted. At present, we have no definitive explanation

for the anomalous Raman spectrum of β - Sb_2Te_3 in Ref. **39**. Maybe this is due to the decrease of the crystalline quality of nanocrystalline Sb_2Te_3 after the α - β phase transition.

C. Raman scattering of γ - Sb_2Te_3 and δ - Sb_2Te_3

Similarly to the previous phase, XRD measurements show that β - Sb_2Te_3 undergoes a phase transition around 12 GPa towards an still unknown phase γ - Sb_2Te_3 . Recent high-pressure XRD experiments have shown the appearance of a new phase beyond β - Sb_2Te_3 at pressures above 15 GPa in nanocrystalline Sb_2Te_3 whose structure was not resolved [**39**]. It has been proposed on the basis of Raman scattering measurements that γ - Bi_2Se_3 , obtained above 20 GPa, is isostructural to γ - Bi_2Te_3 (with C2/c structure) [**34,38**]. Therefore, it is reasonable to assume that γ - Sb_2Te_3 could be also isostructural to γ - Bi_2Te_3 . In **Figure 5(a)** we show the experimental Raman spectra of γ - Sb_2Te_3 at different pressures from 15 GPa up to 26.0 GPa and at room pressure after releasing pressure. We have observed that the Raman spectrum above 14.5 GPa is different from that of the β phase and that above 24.3 GPa the Raman spectrum disappears thus suggesting a phase transition to a Raman-inactive phase. Furthermore, on pressure release we have observed that the sample reverts back to the original rhombohedral phase below 5 GPa after considerable hysteresis. The spectrum of the recovered sample in the rhombohedral phase at 1 atm after releasing pressure is shown as the last spectrum in the top of **Fig. 5(a)**. A similar behavior has been observed in the Raman spectra of Bi_2Te_3 [**48**] and in Bi_2Se_3 [**38**].

It has been recently demonstrated that the second high-pressure phase of Bi_2Te_3 (γ - Bi_2Te_3) at room temperature is a monoclinic C2/c structure [**34**]. In this monoclinic phase Bi atoms occupy an 8f Wyckoff site and Te atoms occupy 8f and 4e Wyckoff sites [**34**]. Group theoretical considerations predict 30 vibrational modes with the following representation [**63**]

$$\Gamma_{30} = (7A_g + 7A_u) + (8B_g + 8B_u). \quad (3)$$

One A_u and two B_u are acoustic modes and the rest are optical modes. Therefore, we expect 15 zone-center Raman-active modes ($7A_g + 8B_g$) for the C2/c phase.

We have marked at the bottom of **Fig. 5(a)** the calculated Raman mode frequencies for the C2/c phase at 15.2 GPa and have compared it with the Raman spectrum at 15.2 GPa. The rather broad bands observed in the experimental spectrum and the fact that many theoretical Raman modes are predicted to be close to each other make difficult the assignment of individual Raman bands to the theoretically predicted Raman modes. In any case, on the light of the similarities of Sb_2Te_3 with Bi_2Te_3 and Bi_2Se_3 , we have attempted an assignment of the different Raman modes to the theoretically expected modes for the C2/c phase.

In our Raman spectrum at 15.2 GPa the highest-frequency mode of $\gamma\text{-Sb}_2\text{Te}_3$ has a smaller frequency (178.5 cm^{-1}) than the highest-frequency mode of $\beta\text{-Sb}_2\text{Te}_3$ (190 cm^{-1}). This decrease in frequency of the highest-frequency mode suggests an increase in the Sb-Te distance related to an increase of the Sb coordination from sevenfold in $\beta\text{-Sb}_2\text{Te}_3$ to eightfold in $\gamma\text{-Sb}_2\text{Te}_3$. This increase of Sb coordination in the $\beta\text{-}\gamma$ transition is in good agreement with the recently observed increase of the Bi coordination on going from $\beta\text{-Bi}_2\text{Te}_3$ to $\gamma\text{-Bi}_2\text{Te}_3$ [34,48] and $\beta\text{-Bi}_2\text{Se}_3$ to $\gamma\text{-Bi}_2\text{Se}_3$ [38].

A decomposition of the Raman spectrum at 18.6 GPa into Voigt profiles is shown in Fig. 2 of the supplementary material [62]. With this decomposition we have tentatively assigned 10 of the 13 Raman active modes expected above 50 cm^{-1} . Note that at least 9 bands can be clearly observed without fitting the Raman spectrum. **Figure 5(b)** shows the pressure dependence of the experimental and theoretical Raman mode frequencies in $\gamma\text{-Sb}_2\text{Te}_3$. It can be observed that there is a consistent agreement between the experimental and theoretical Raman mode frequencies and its pressure coefficients. Therefore, we can reasonably assume that the $\gamma\text{-Sb}_2\text{Te}_3$ phase has the monoclinic C2/c structure already found in Bi_2Te_3 and Bi_2Se_3 . **Table IV** summarizes the experimental and theoretical first-order Raman mode frequencies and pressure coefficients at 15.2 GPa in the $\gamma\text{-Sb}_2\text{Te}_3$ phase. In our experiments, we have not observed the two lowest frequency modes (B_g^1 and A_g^1) because they could be modes with weak intensity and whose frequencies are below the cutting edge of the Raman edge filter of our spectrometer. Furthermore, in the region where the A_g^3 mode should be located, calculated to be 106 cm^{-1} at 18.6 GPa, we obtain from the decomposition in Voigt profiles a broad band whose frequency is around 91 cm^{-1} and it is difficult to follow at high pressures. We think that this band could be attributed to a second-order Raman mode while the A_g^3 mode could not be detected because of its weak intensity since it

should be observed in a frequency region where overlapping with other modes should not occur. As regards the high-frequency region, we have found a mode close to 155 cm^{-1} that could be assigned to the B_g^6 or B_g^7 mode. We have decided to assign this band to the B_g^6 mode because it is close in frequency and pressure coefficient to the parameters theoretically calculated for the B_g^6 mode at least in the low-pressure range. Note that as pressure increases and the phase transition approaches near 24.5 GPa there is some dispersion with experimental data for this mode. Taking into account the previous assignment we consider that the B_g^7 mode could have been not detected due to its weak intensity because it is located on the broad high-frequency shoulder of the B_g^6 mode. The highest frequency mode that has been measured at about 178 cm^{-1} at 15.2 GPa could be assigned to the A_g^7 or B_g^8 mode. This mode is assigned to the B_g^8 one because its proximity in frequency with the *ab initio* results for the B_g^8 mode in comparison to the *ab initio* results for the A_g^7 mode. Probably the A_g^7 mode is a weak mode very close in frequency to the B_g^8 mode that is masked by the intensity of the B_g^8 peak.

As already commented, we have detected a lack of Raman scattering signal above 24.5 GPa thus suggesting a phase transition to a Raman-inactive phase above that pressure. The lack of Raman scattering above this pressure indicates that $\gamma\text{-Sb}_2\text{Te}_3$ undergoes a complete phase transition towards $\delta\text{-Sb}_2\text{Te}_3$, and it suggests that the nature of the new phase could be the disordered bcc structure with Im-3m space group recently found in Bi_2Te_3 above 14.4 GPa which dominates the x-ray diffraction spectrum above 25 GPa [33,34] and that also seems to be the case in Bi_2Te_3 above 22 GPa [48] and in Bi_2Se_3 above 28 GPa [38]. Our measurements suggest that, similarly to the other compounds of this family of semiconductors, there is no phase transition in Sb_2Te_3 to the monoclinic bcc-like C2/m phase with nine/ten Sb coordination. Note that the main difference between the similar bcc-like C2/m and disordered bcc (Im-3m) structures is that the bcc-like C2/m phase is Raman active, with 12 Raman-active modes, while the Im-3m phase is Raman inactive. However, we cannot fully assign $\delta\text{-Sb}_2\text{Te}_3$ to the disordered bcc structure because: i) it is possible that the Raman scattering signal of the bcc-like C2/m phase is very weak and we have not been able to measure it; or ii) the $\delta\text{-Sb}_2\text{Te}_3$ phase could be another Raman-inactive phase; i.e., a disordered fcc structure.

In order to study the structural stability of the different phases of Sb_2Te_3 and to support the previous assignments of the different high-pressure phases of Sb_2Te_3 we have performed total-energy calculations for Sb_2Te_3 with the structures observed in

Bi₂Te₃ at different pressures [33,34]. **Figure 6(a) and (b)** show the energy vs. volume and the Gibbs free energy difference at 300 K vs. pressure for the different phases calculated. In **Fig. 6(a)** it can be observed that the different phases observed in Bi₂Te₃ under pressure [34] cross each other at reduced volumes and therefore are candidates to be observed also in Sb₂Te₃ at different pressures as already happens for phase C2/m observed by XRD experiments in Sb₂Te₃ [39]. Therefore, our assignments of the peak frequencies in the preceding paragraphs to the proposed phases are consistent. The only doubt is whether δ -Sb₂Te₃ is the bcc-like C2/m nine/ten phase or a disordered bcc or fcc phase. Our calculations support the phase transition from the C2/c phase towards the bcc-like C2/m phase, but we have not been able to make calculations for the disordered bcc phase with Im-3m space group. Therefore, in order to fully ensure that these phases are consistent we have plotted in **Figure 6(b)** the pressure dependence of the Gibbs free energy difference at T = 300 K for the different monoclinic phases with respect to the R-3m, which is taken as reference. The calculated phase-transition pressure for the R-3m to the C2/m phase is 6.9 GPa, which compares nicely with the experimental value (7.7 GPa). The calculated phase-transition pressure for the C2/m to the C2/c phase is 12.3 GPa in good agreement with the experimental value (14.5 GPa). As regards the last phase transition, our calculations show that the monoclinic bcc-like C2/m nine-ten structure does not cross below the C2/c structure near or above 20 GPa; thus, it is less stable than the C2/c phase above 20 GPa. This means that even at T=0K a possible C2/c to bcc-like C2/m nine/ten phase transition is suggested by the energy-volume plot, when one accounts for the Gibbs free energy at room temperature that phase transition is not probable. Therefore, we conclude that it is likely that the δ -Sb₂Te₃ phase is a disordered bcc phase with Im-3m structure as already found in Bi₂Te₃ (a disordered fcc phase cannot be excluded as already mentioned) since it is expected that the Gibbs free energy of the disordered bcc structure is lower than that of the bcc-like C2/m phase. Finally, we must comment that it is possible that the phase transition from the C2/c to the Im-3m phase begins at much lower pressure than 25 GPa but Raman scattering cannot detect it because of the lack of Raman scattering of the latter phase.

V. Conclusions

We have performed room-temperature Raman scattering measurements and *ab initio* total-energy and lattice dynamics calculations in Sb₂Te₃ up to 26 GPa. Our results suggest that Sb₂Te₃ could exhibit the same sequence of pressure-induced phase

transitions up to 26 GPa as Bi_2Te_3 and Bi_2Se_3 : from rhombohedral R-3m structure (α - Sb_2Te_3) to the C2/m phase (β - Sb_2Te_3), from the C2/m phase to the C2/c structure (γ - Sb_2Te_3), and from the C2/c structure to a disordered bcc structure (δ - Sb_2Te_3). Our hypothesis is justified by the similar Raman spectra and XRD patterns of the three compounds under pressure. The nature of these high-pressure phases has been measured by means of XRD in Bi_2Te_3 [33,34] and in the case of the β phase also in Bi_2Se_3 [38] and in Sb_2Te_3 [39]. It has also been confirmed by Raman measurements in the three compounds (Bi_2Te_3 [48], Bi_2Se_3 [38], and Sb_2Te_3 [this work]). The pressure dependence of the experimental Raman and infrared mode frequencies in the different phases is reported and the Raman modes are in general good agreement with theoretical calculations.

Furthermore, we have found Raman anomalies and a change of behavior in the c/a ratio vs. pressure plot that seem to confirm that an electronic topological transition occurs in the rhombohedral phase of Sb_2Te_3 around 3-3.5 GPa, as reported in Ref. 31. This ETT occurs in Sb_2Te_3 at a similar pressure than Bi_2Te_3 [34,37,48] and at slightly smaller pressures than in Bi_2Se_3 [38]. Finally, on fully releasing the pressure Sb_2Te_3 returns to the rhombohedral structure below 5 GPa in a similar way than already found for Bi_2Te_3 and Bi_2Se_3 . We hope the present work will further stimulate new x-ray diffraction measurements in Sb_2Te_3 under high pressure to fully confirm the structures here discussed. Finally, we want to stress that more work on layered chalcogenide compounds is needed to understand the mechanism of their pressure-induced electronic topological phase transitions and the subtle effects on their structures and properties.

Acknowledgments

This work has been done under financial support from Spanish MICINN under projects MAT2010-21270-C04-03/04, and CSD-2007-00045 and supported by the Ministry of Education, Youth and Sports of the Czech Republic (MSM 0021627501). E P-G acknowledges the financial support of the Spanish MEC under a FPI fellowship. Supercomputer time has been provided by the Red Española de Supercomputación (RES) and the MALTA cluster.

References

- [1] G.J. Snyder and E.S. Tobere, *Nat. Mater.* **7**, 105 (2008).
- [2] T.S. Kim, B.S. Chun, J.K. Lee, H. G. Jung, 12th International Symposium on Metastable and Nano-Materials (ISMANAM-2005), Paris, France, July 03-07, 2005; pp 710-713.
- [3] R. Venkatasubramanian, E. Siivola, T. Colpitts, B. O'Quinn, *Nature* **413**, 597 (2001).
- [4] T.C. Harman, P.J. Taylor, M.P. Walsh, B.E. LaForge, *Science* **297**, 2229(2002).
- [5] J. Chen, T. Sun, D.H. Sim, H.Y. Peng, H.T. Wang, S.F. Fan, H.H. Hng, J. Ma, F.Y.C Boey, S. Li, M.K. Samani, G.C.K. Chen, X.D. Chen, T. Wu, and Q.Y. Yan, *Chem. Mat.* **22**, 3086 (2010).
- [6] Y. Yin, H. Sone, and S. Hosaka, *J. Appl. Phys.* **102**, 064503 (2007).
- [7] M.S. Kim, S.H. Cho, S.K. Hong, J.S. Roh, and D.J. Choi, *Ceram. Int.* **34**, 1043 (2008).
- [8] T.L. Anderson and H.B Krause, *Acta Crystallogr., Sect. B: Struct. Crystallogr. Cryst. Chem.* **30**, 1307 (1974).
- [9] H. Zhang, C.X. Liu, X.L. Qi, X. Dai, Z. Fang, and S.C. Zhang, *Nature Phys.* **5**, 438 (2009).
- [10] M.Z. Hassan and C.L. Kane, *Rev. Mod. Phys.* **82**, 3045 (2010).
- [11] J.E. Moore, *Nature* **464**, 194 (2010).
- [12] Y. Xia, D. Qian, D. Hsieh, L. Wray, A. Pal, H. Lin, A. Bansil, D. Grauer, y.S. Hor, R.J. Cava, and M.Z. Hassan, *Nat. Phys.* **5**, 398 (2009).
- [13] H. Zhang, C.X. Liu, X.L. Qi, X. Dai, Z. Fang, and S.C. Zhang, *Nat. Phys.* **5**, 438 (2009).
- [14] G. Wang, and T. Cagin, *Phys. Rev. B* **76**, 075201 (2007).
- [15] Y.L. Chen, J.G. Analytis, J.H. Chu, Z.K. Liu, S.K. Mo, X.L. Qi, H.J. Zhang, D.H. Lu, X. Dai, Z. Fang, S.C. Zhang, I.R. Fisher, Z. Hussain, and Z.X. Shen, *Science* **325**, 178 (2009).
- [16] J.V. Badding, J.F. Meng, D.A. Polvani, *Chem. Mater.* **10**, 2889 (1998).
- [17] D.A. Polvani, J.F. Meng, N.V. Chandra Shekar, J. Sharp, and J.V. Badding, *Chem. Mater.* **13**, 2068 (2001).
- [18] N.V. Chandra Shekar, D.A. Polvani, J.F. Meng, and J.V. Badding, *Physica B* **358**, 14 (2005).

- [19] S.V. Ovsyannikov, V.V. Shchennikov, G.V. Vorontsov, A.Y. Manakov, A.Y. Likhacheva, and V.A. Kulbachinskii, *J. Appl. Phys.* **104**, 053713 (2008).
- [20] S.V. Ovsyannikov and V.V. Shchennikov, *Chem. Mater.* **22**, 635 (2010).
- [21] C.-Y. Li, A.L. Ruoff, and C.W. Spencer, *J. Appl. Phys.* **32**, 1733 (1961).
- [22] L.F. Vereshchagin, E.Ya. Atabaeva, and N.A. Bedeliani, *Sov. Phys. Solid State* **13**, 2051 (1972).
- [23] L.G. Khvostantsev, A.I Orlov, N. Kh. Abrikosov, and L.D. Ivanova, *Phys. Stat. Solidi a* **58**, 37 (1980).
- [24] N. Sakai, T. Kajiwara, K. Takemura, S. Minomura, and Y. Fujii, *Solid State Commun.* **40**, 1045 (1981).
- [25] L.G. Khvostantsev, A.I Orlov, N. Kh. Abrikosov, and L.D. Ivanova, *Phys. Stat. Solidi a* **89**, 301 (1985).
- [26] M. Bartkowiak and G.D. Mahan, 18th International Conference on Thermoelectrics, IEEE 713 (1999).
- [27] T. Thonhauser, T.J. Scheidemantel, J.O. Sofo, J.V. Badding, and G.D. Mahan, *Phys. Rev. B* **68**, 085201 (2003).
- [28] T. Thonhauser, *Solid State Commun.* **129**, 249 (2004).
- [29] M. Einaga, Y. Tanabe, A. Nakayama, A. Ohmura, F. Ishikawa, and Yuh Yamada, *J. Phys.: Conf. Ser.* **215**, 012036 (2010).
- [30] J.L. Zhang, S.J. Zhang, H.M. Weng, W. Zhang, L.X. Yang, Q.Q. Liu, S.M. Feng, X.C. Wang, R.C. Yu, L.Z. Cao, L. Wang, W.G. Yang, H.Z. Liu, W.Y. Zhao, S.C. Zhang, X. Dai, Z. fang, and C.Q. Jin, *Proc. Nat. Acad. Sci.* **108**, 24 (2011).
- [31] M.K. Jacobsen, R.S. Kumar, A.L. Cornelius, S.V. Sinogeiken, and M.F. Nicol, *AIP Conf. Proc.* **955**, 171 (2007).
- [32] A. Nakayama, M. Einaga, Y. Tanabe, S. Nakano, F. Ishikawa, and Y. Yamada, *High. Press. Res.* **29**, 245 (2009).
- [33] M. Einaga, A. Ohmura, A. Nakayama, F. Ishikawa, Y. Yamada, and S. Nakano, *Phys. Rev. B* **83**, 092102 (2011).
- [34] L. Zhu, H. Wang, Y.C. Wang, J. Lv, Yanmei Ma, Q.L. Cui, Yanming Ma, and G.T. Zou, *Phys. Rev. Lett.* **106**, 145501 (2011).
- [35] E.S. Itskevich, L.M. Kashirskaya, and V.F. Kraidenov, *Semicond.* **31**, 276 (1997).
- [36] V.V. Sologub, M.L. Shubnikov, E.S. Itskevich, L.M. Kashirskaya, R.V. Parfen'ev, and A.D. Goletskaya, *Zh. Eksp. Teor. Fiz.* **79**, 2374 (1980) [*Sov. Phys. JETP* **52**, 1203 (1980)].

- [37] A. Polian, M. Gauthier, S.M. Souza, D.M. Trichês, J. Cardoso de Lima, and T.A. Grandi, *Phys. Rev. B* **83**, 113106 (2011).
- [38] R. Vilaplana, D. Santamaría-Pérez, O. Gomis, F.J. Manjón, J. González, A. Segura, A. Muñoz, P. Rodríguez-Hernández, E. Pérez-González, V. Marín-Borrás, V. Muñoz-Sanjose, C. Drasar, and V. Kucek, accepted in *Phys. Rev. B* (2011).
- [39] S. M. de Souza, D. M. Trichês, C. M. Poffo, J. Cardoso de Lima, T.A. Grandi, A. Polian and M. Gauthier, arXiv:1105.1097v1 (2011).
- [40] I.M. Lifshitz, *Sov. Phys. JETP* **11**, 1130 (1960).
- [41] W. Richter, H. Köhler, and C.R. Becker, *Phys. Stat. Solidi b* **84**, 619 (1977).
- [42] G.C. Sosso, S. Caravati, and M. Bernasconi, *J. Phys.: Condens. Matter* **21**, 095410 (2009).
- [43] L. Dagens, *J. Phys. F: Met. Phys.* **8**, 4496 (1978).
- [44] L. Dagens and C. Lopez-Rios, *J. Phys. F: Met. Phys.* **9**, 2195 (1979).
- [45] A.F. Goncharov, V.V. Struzhkin, *Physica B* **385**, 117 (2003).
- [46] D. Antonangeli, D.L. Farber, A.H. Said, L.R. Benedetti, C.M. Aracne, A. Landa, P. Söderlind, and J.E. Klepeis, *Phys. Rev. B* **82**, 132101 (2010).
- [47] D. Santamaria-Perez, A. Vegas, C. Muehle, and M. Jansen, *J. Chem. Phys.* **135**, 054511 (2011).
- [48] R. Vilaplana, O. Gomis, F.J. Manjón, A. Segura, E. Pérez-González, P. Rodríguez-Hernández, A. Muñoz, J. González, V. Marín-Borrás, V. Muñoz-Sanjose, C. Drasar, and V. Kucek, *Phys. Rev. B* **84**, 104112 (2011).
- [49] P. Larson, *Phys. Rev. B* **74**, 205113 (2006).
- [50] P. Lošťák, L. Beneš, S. Civiš, and H. Süßmann, *J. Mater. Sci.* **25**, 277 (1990).
- [51] J. Horák, P.C. Quayle, J.S. Dyck, Č. Drašar, P. Lošťák, and C. Uher, *J. Appl. Phys.* **103**, 013516 (2008).
- [52] G.J. Piermarini, S. Block, and J.D. Barnett, *J. Appl. Phys.* **44**, 5377 (1973).
- [53] D. Errandonea, Y. Meng, M. Somayazulu, and D. Hausermann, *Physica B* **355**, 116 (2005).
- [54] K. Syassen, *High Press. Res.* **28**, 75 (2008).
- [55] P. Hohenberg and W. Kohn, *Phys. Rev.* **136**, 3864 (1964).
- [56] G. Kresse and J. Hafner, *Phys. Rev. B* **47**, 558 (1993); *ibid* **49**, 14251(1994); G. Kresse and J. Furthmüller, *Comput. Mat. Sci.* **6**, 15 (1996); G. Kresse and J. Furthmüller, *Phys. Rev. B* **54**, 11169 (1996).

- [57] P. E. Blöchl, Phys. Rev. B **50**, 17953 (Dec 1994). G. Kresse and D. Joubert, Phys. Rev. B **59**, 1758 (1999).
- [58] J. P. Perdew, A. Ruzsinszky, G. I. Csonka, O.A. Vydrov, G.E. Suseria, L.A. Constantin, X Zhou and K. Burke, Phys. Rev. Lett. **100**, 136406 (2008).
- [59] A. Mujica, A. Rubio, A. Muñoz, and R. J. Needs, Rev. Mod. Phys. **79**, 863 (2003).
- [60] M.A. Blanco, E. Francisco, V. Luaña, Computer Physics Communications **158**, 57 (2004).
- [61] K. Parlinski, computer code PHONON. See: <http://wolf.ifj.edu.pl/phonon>.
- [62] See EPAPS Document No. [] for calculation details regarding IR-active modes.
- [63] G. Herzberg, Molecular Spectra and Molecular Structure II: Infra-Red and Raman Spectra (D. Van Nostrand Co. Inc., New York, 1945).
- [64] M. Cardona, High Press. Res. **24**, 17 (2004); idem, phys. stat. sol (b) **341**, 3128 (2004).
- [65] C. Ulrich, M.A. Mroginiski, A.R. Goñi, A. Cantarero, U. Schwarz, V. Muñoz, and K. Syassen, phys. stat. sol. (b) **198**, 121 (1996).
- [66] A.M. Kubelikov, H.P. Olijnyk, A.P. Jephcoat, Z.Y. Salaeva, S. Onari, and K.R. Allakverdiev, phys. stat. sol (b) **235**, 517 (2003).
- [67] W. Chen and S.F. Ren, Phys. Rev. B **83**, 094301 (2011).
- [68] S.G. Buda, N.R. Serebryanaya, G.A. Dubitskiy, E.E. Semenova, V.V. Aksenenkov, and V.D. Blanck, High Press. Res. **31**, 86 (2011).

Table I. Calculated (th.) and experimental (exp.) lattice parameters, bulk modulus (B_0), and its derivative (B_0') of Sb_2Te_3 in the R-3m (α) structure at ambient pressure, and calculated structural parameters of Sb_2Te_3 in the C2/m (β) and C2/c (γ) structures at 8.6 and 15.2 GPa, respectively.

	a(Å)	b(Å)	c(Å)	β (°)	B_0 (GPa)	B_0'	Reference
α - Sb_2Te_3 (0 GPa)							
th.(GGA-PBEsol)	4.276		29.940		41.0	5.2	This work
th.(GGA-PBE)	4.316		31.037				36
th.(GGA-PBE)	4.350		30.844				27
th.(GGA-PBE)	4.440		30.29				14
exp.	4.264		30.458				8
exp.	4.262		30.450		40	4.0*	24
exp.	4.265		30.450		30.2	9.4	31
exp.	4.275		30.400		40.6	5.1	39
β - Sb_2Te_3 (8.6 GPa)							
th.(GGA-PBEsol)	14.531	4.019	8.972	90.47	34.74	5.0	This work
γ - Sb_2Te_3 (15.2 GPa)							
th.(GGA-PBEsol)	9.669	6.895	7.544	70.81	38.91	4.5	This work

* fixed

Table II. Experimental room-temperature Raman-mode frequencies and pressure coefficients observed in α -Sb₂Te₃ at both room pressure and 4.0 GPa, as obtained from fits to the data using $\omega(P) = \omega(P_0=1 \text{ atm}) + a_1 \cdot (P-P_0)$ and $\omega(P) = \omega(P_0=4 \text{ GPa}) + a_1 \cdot (P-P_0)$, respectively. Theoretical (th.) values are also shown for comparison and fitted either to a linear or quadratic expression.

Mode	$\omega(P_0)$ (cm ⁻¹)	a_1 (cm ⁻¹ /GPa)	$\omega(P_0)$ (th.) (cm ⁻¹)	a_1 (th.) (cm ⁻¹ /GPa)	a_2 (th.) (cm ⁻¹ /GPa ²)
E _g ¹			50.4	2.62	-0.09
A _{1g} ¹	68.4(5) ^a	4.5(1) ^a	68.9	4.3	-0.07
	85.0(3) ^b	3.1(1) ^b			
E _g ²	110.9(8) ^a	3.6(1) ^a	116.6	2.11	
	124.3(4) ^b	2.52(8) ^b			
A _{1g} ²	165.0(8) ^a	3.0(2) ^a	167.6	2.57	
	176.6(5) ^b	2.5(1) ^b			

^a Estimated at room pressure ($P_0 = 1 \text{ atm}$).

^b Estimated at $P_0 = 4.0 \text{ GPa}$.

Table III. Experimental Raman-mode frequencies and pressure coefficients observed in β -4Sb₂Te₃ at room temperature at $P_0 = 8.6$ GPa as obtained from fits using $\omega(P) = \omega(P_0) + a_1 \cdot (P - P_0)$. Theoretical (th.) *ab initio* values for the frequencies and pressure coefficients at 8.6 GPa are also shown for comparison.

Mode	$\omega(P_0)$ (cm ⁻¹)	a_1 (cm ⁻¹ /GPa)	$\omega(P_0)$ (th.) (cm ⁻¹)	a_1 (th.) (cm ⁻¹ /GPa)
B _g ¹			23.8	-1.29
A _g ¹			46.1	-0.50
A _g ²	68(3)	1.02(3)	61.6	1.52
B _g ²	71(2)	1.67(9)	61.9	1.58
A _g ³	78(2)	0.79(7)	74.6	0.42
A _g ⁴	94(2)	2.70(7)	98.4	2.20
B _g ³	105(2)	1.6(2)	103.8	1.06
B _g ⁴	111(3)	2.2(1)	116.9	2.16
A _g ⁵	118(3)	2.16(9)	117.9	1.77
B _g ⁵	118(3)	2.16(9)	121.7	1.68
A _g ⁶	124(3)	2.7(2)	122.2	2.16
A _g ⁷	140(2)	2.23(8)	143.0	2.18
A _g ⁸	150(3)	2.49(7)	147.7	2.76
A _g ⁹	166(2)	1.25(4)	164.2	1.36
A _g ¹⁰	171(2)	2.9(1)	173.0	2.22

Table IV.

Experimental Raman-mode frequencies and pressure coefficients observed in γ -Sb₂Te₃ at room temperature at $P_0=15.2$ GPa as obtained from fits using $\omega(P) = \omega(P_0) + a_1 \cdot (P - P_0)$. Theoretical (th.) *ab initio* values for the frequencies and pressure coefficients at 15.2 GPa are also shown for comparison.

Mode	$\omega(P_0)$ (cm ⁻¹)	a_1 (cm ⁻¹ /GPa)	$\omega(P_0)$ (th.) (cm ⁻¹)	a_1 (th.) (cm ⁻¹ /GPa)
B _g ¹			37.4	0.40
A _g ¹			47.4	1.00
B _g ²	63(5)	-0.05(2)	59.5	0.20
A _g ²	70(4)	0.43(4)	76.2	0.69
B _g ³	74(4)	0.01(1)	77.6	0.06
A _g ³			96.4	2.63
B _g ⁴	121(7)	1.34(7)	119.4	1.11
B _g ⁵	127(6)	1.4(1)	132.0	1.29
A _g ⁴	134(5)	1.44(8)	134.4	1.24
A _g ⁵	141(4)	1.24(5)	140.5	1.10
A _g ⁶	148(5)	1.8(1)	150.4	2.24
B _g ⁶	155(5)	2.38(8)	151.3	2.66
B _g ⁷			162.6	2.32
A _g ⁷			171.1	2.41
B _g ⁸	179(4)	2.32(8)	175.8	2.74

Figure captions

Fig. 1. Experimental Raman spectra of α -Sb₂Te₃ at pressures between 1 atm and 7.7 GPa.

Fig 2. (Color online) (a) Experimental pressure dependence of the Raman mode frequencies in α -Sb₂Te₃. Solid (dashed-dotted) curves represent *ab initio* calculated mode frequencies of modes observed (not observed) in our measurements. Dashed lines represent a different behaviour of the experimental Raman mode with pressure. Error bars for experimental data are smaller or equal than experimental data points. (b) Experimental pressure dependence of the full width half medium (FWHM) of the Raman modes. Solid lines represent two different behaviour of the FWHM with pressure.

Fig. 3. (Color online) (a) Lattice parameters vs. pressure for α -Sb₂Te₃ obtained from *ab initio* calculations (filled circles) and experimental data from Sakai *et al.* [24] (empty squares) and from Souza *et al.* [39] (empty up triangles). Inset: Evolution of the *c/a* ratio vs. pressure for the previous theoretical and experimental data. (b) Unit-cell volume vs. pressure dependence from *ab initio* calculations (filled circles), Sakai *et al.* measurements [24] (empty squares), Souza *et al.* measurements [39] (empty up triangles), and Jacobsen *et al.* measurements [31] (empty down triangles). Solid line represents the Birch-Murnaghan EOS fit for the *ab initio* data.

Fig. 4. (Color online) (a) Experimental Raman spectra of β -Sb₂Te₃ at pressures between 8.6 and 14.5 GPa. Bottom marks indicate the calculated frequencies of the Raman-active modes in the β -Sb₂Te₃ phase at 8.6 GPa. (b) Experimental pressure dependence of the Raman mode frequencies in β -Sb₂Te₃. Solid (dashed-dotted) curves represent *ab initio* calculated mode frequencies of modes observed (not observed) in our measurements.

Fig. 5. (Color online) (a) Experimental Raman spectra of γ -Sb₂Te₃ at pressures between 15.2 and 26 GPa and at ambient pressure after releasing pressure. Bottom marks indicate the calculated frequencies of the Raman-active modes in the γ -Sb₂Te₃ phase at

15.2 GPa. (b) Experimental pressure dependence of the Raman mode frequencies in γ - Sb_2Te_3 . Solid (dashed-dotted) curves represent *ab initio* calculated mode frequencies of modes observed (not observed) in our measurements.

Fig. 6. Theoretical results of energy as a function of volume for $T=0$ K (a), and Gibbs free energy difference as a function of pressure at 300 K (b) for the R-3m, C2/m, C2/c, and bcc-like C2/m phases of Sb_2Te_3 . Free energy of R-3m phase is taken as reference in (b).

Fig. 1

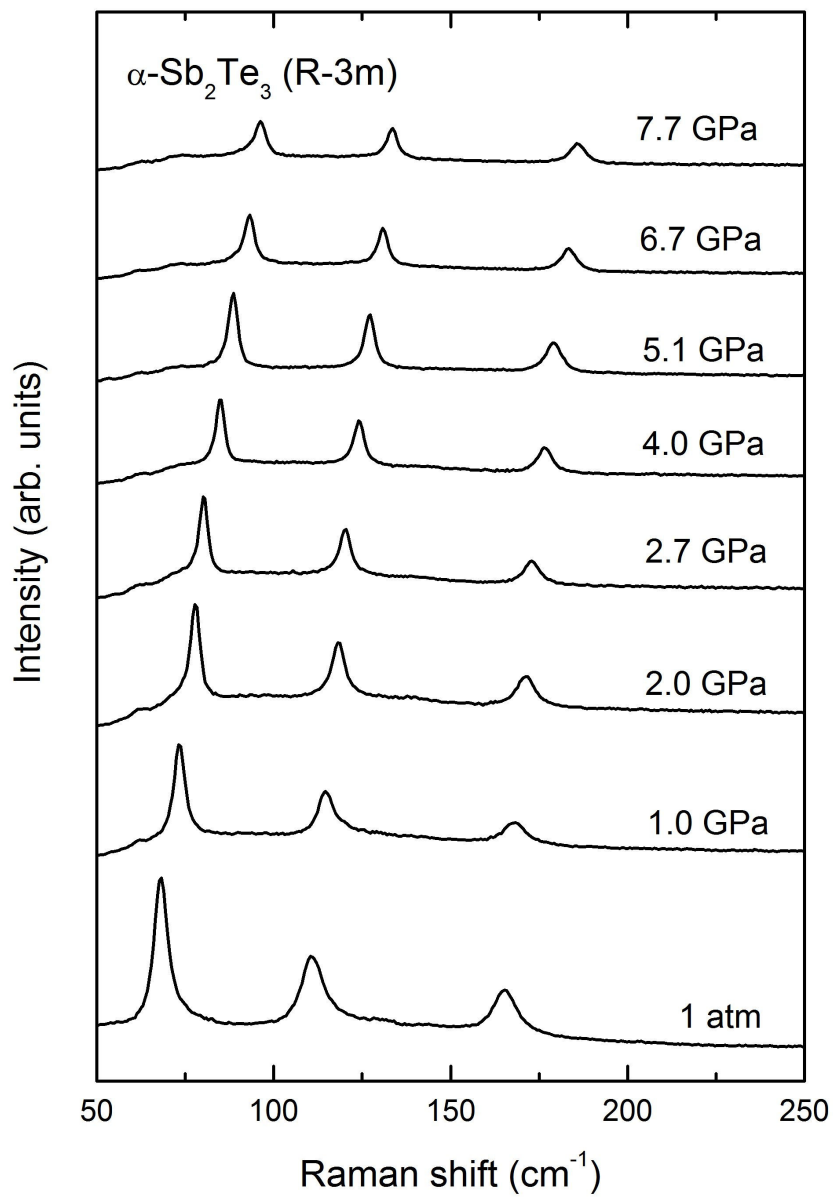


Fig. 2(a)

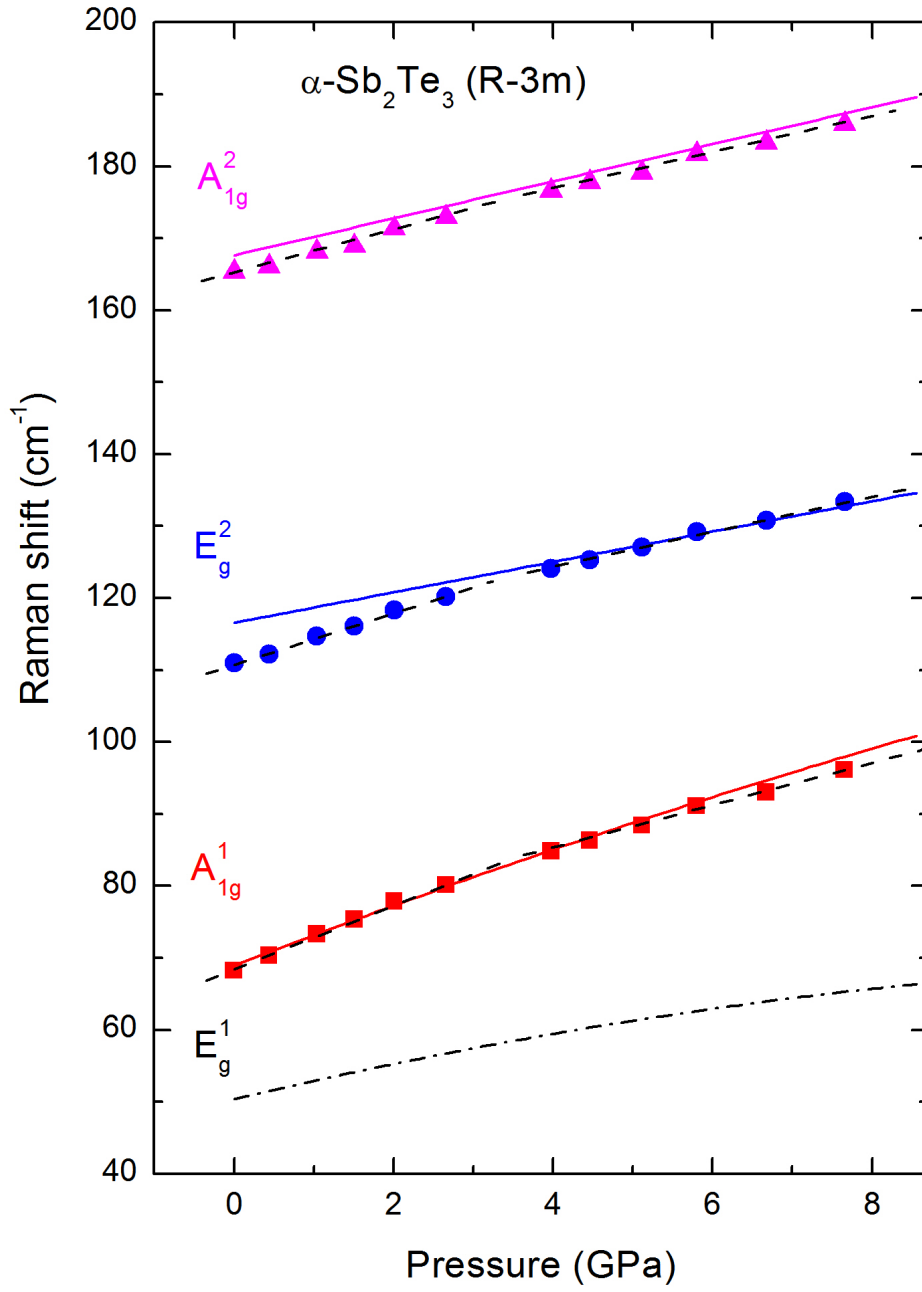


Fig. 2(b)

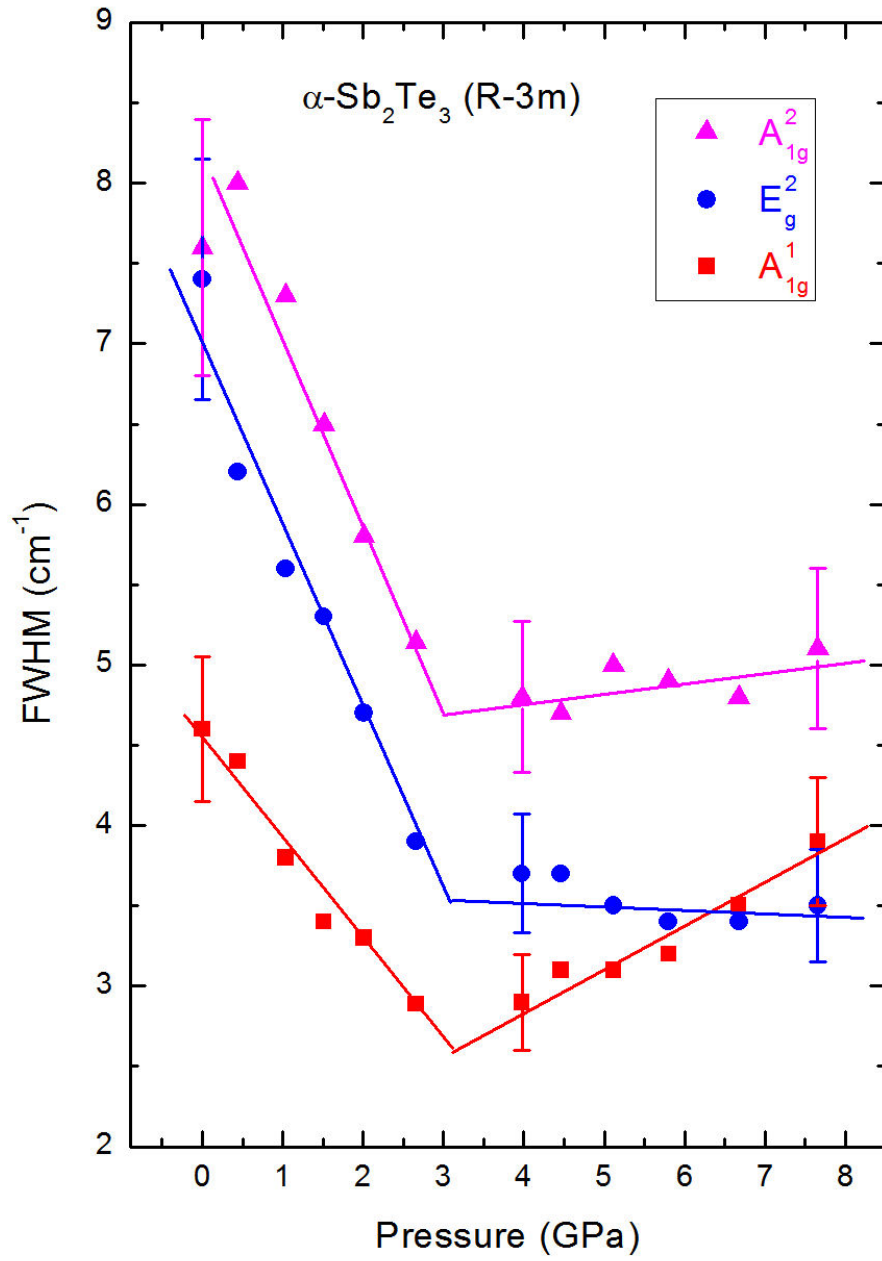


Fig. 3

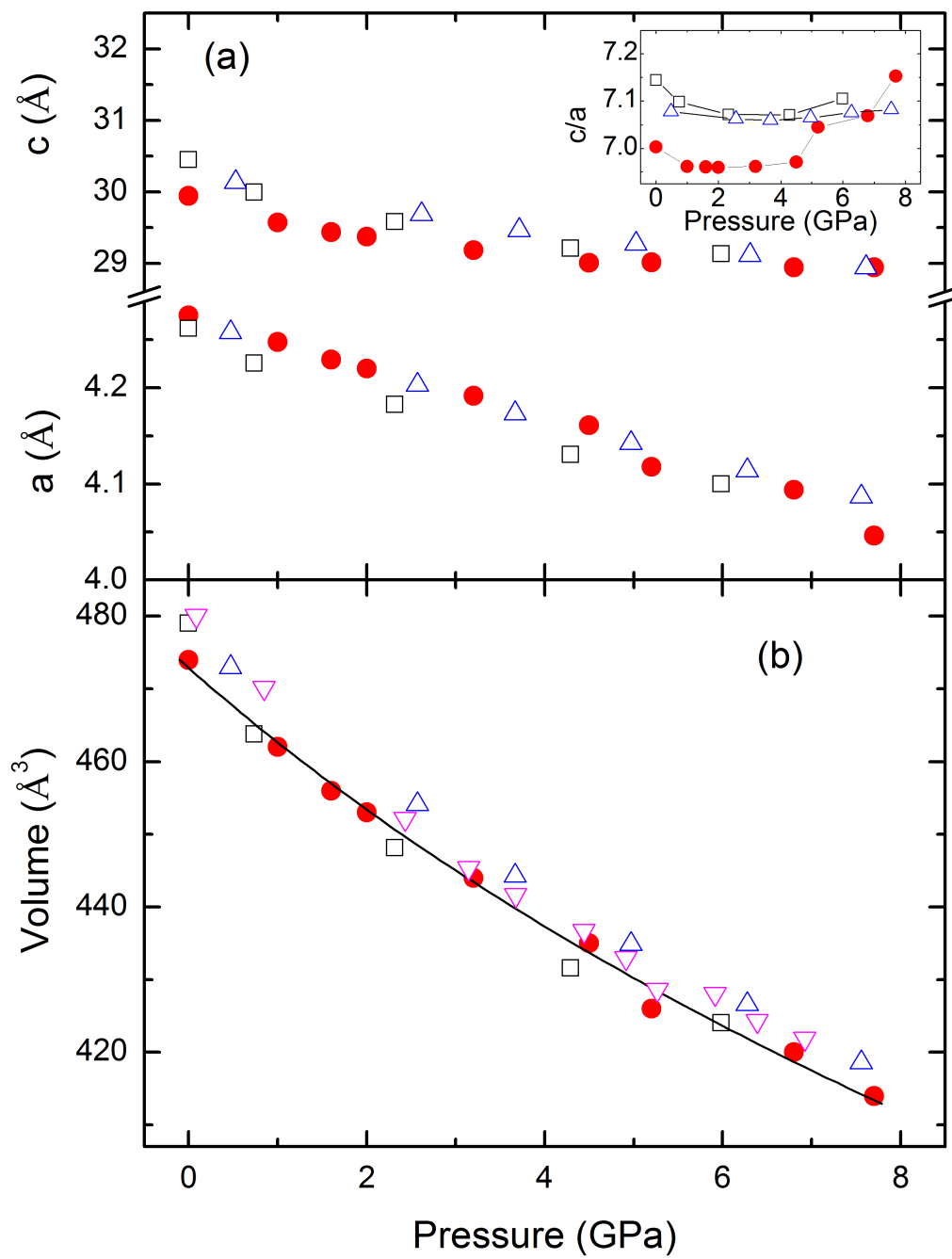


Fig. 4(a)

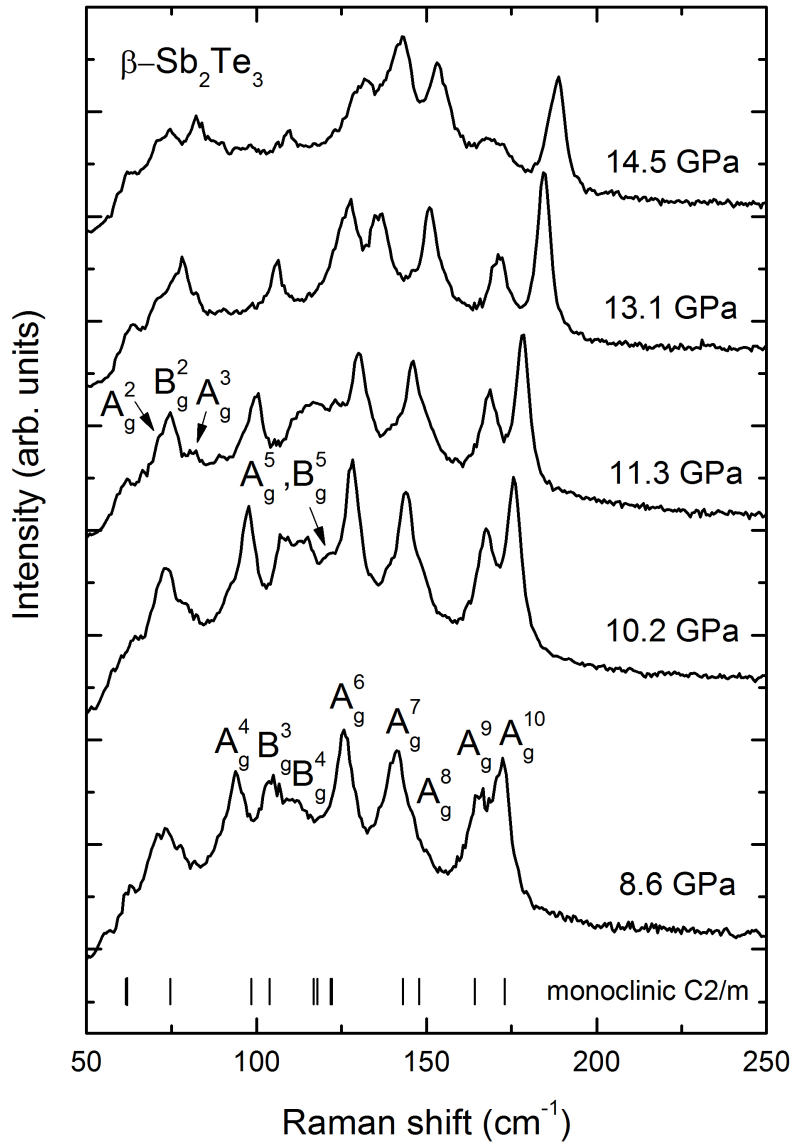


Fig. 4(b)

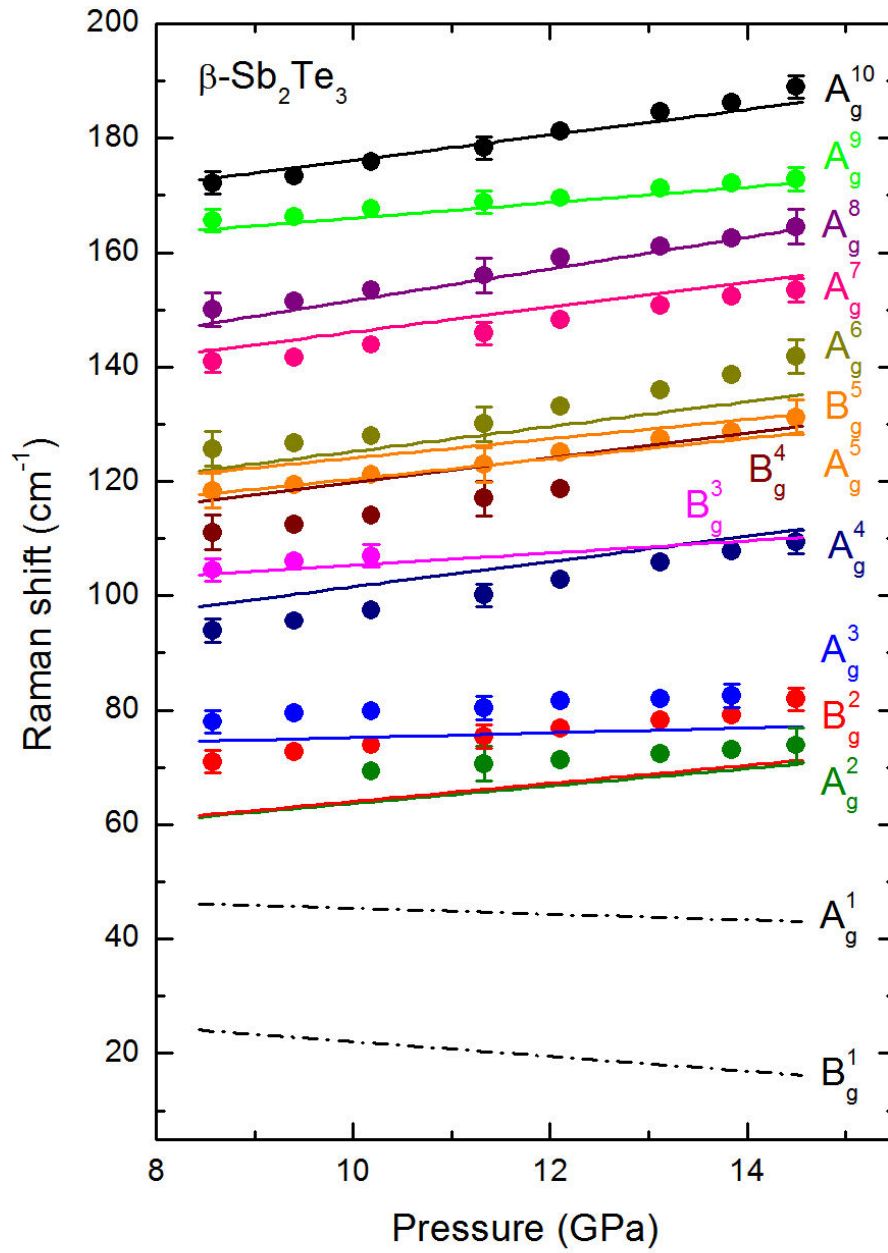


Fig. 5(a)

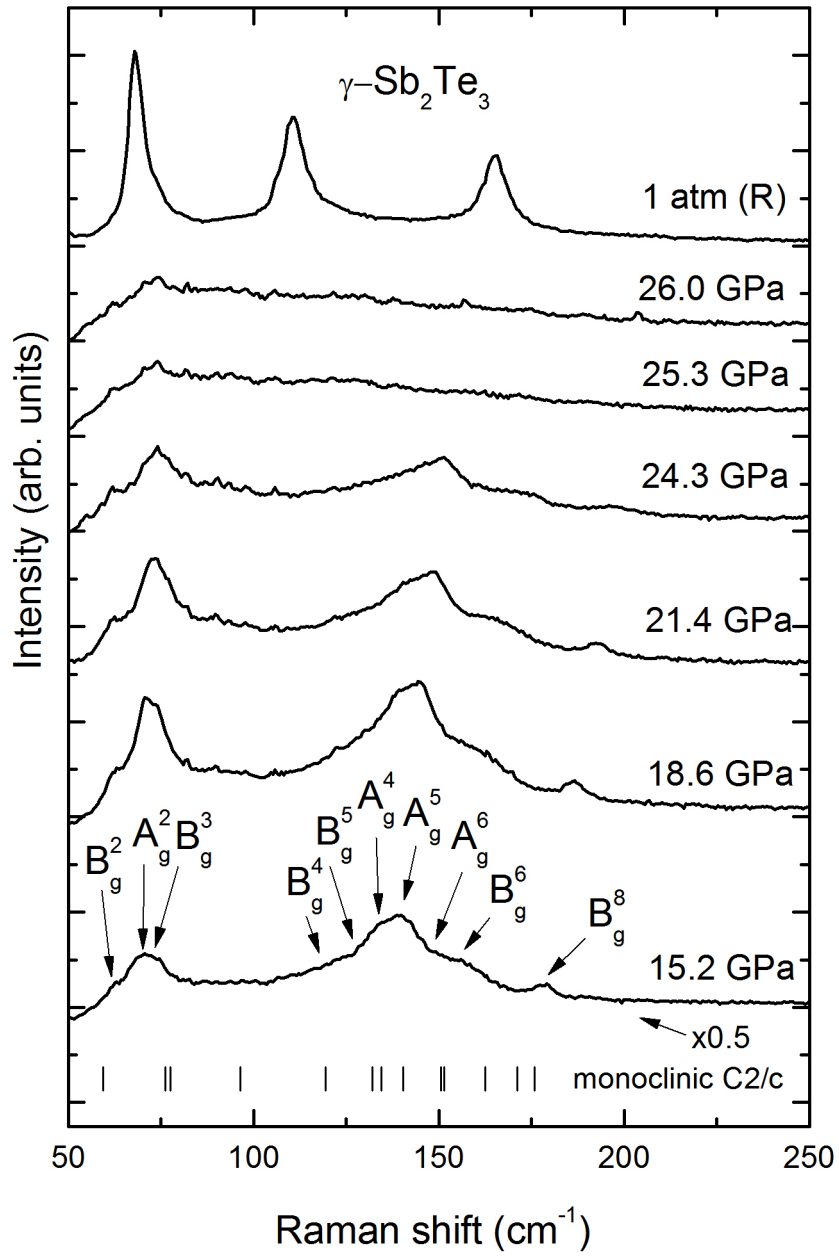


Fig. 5(b)

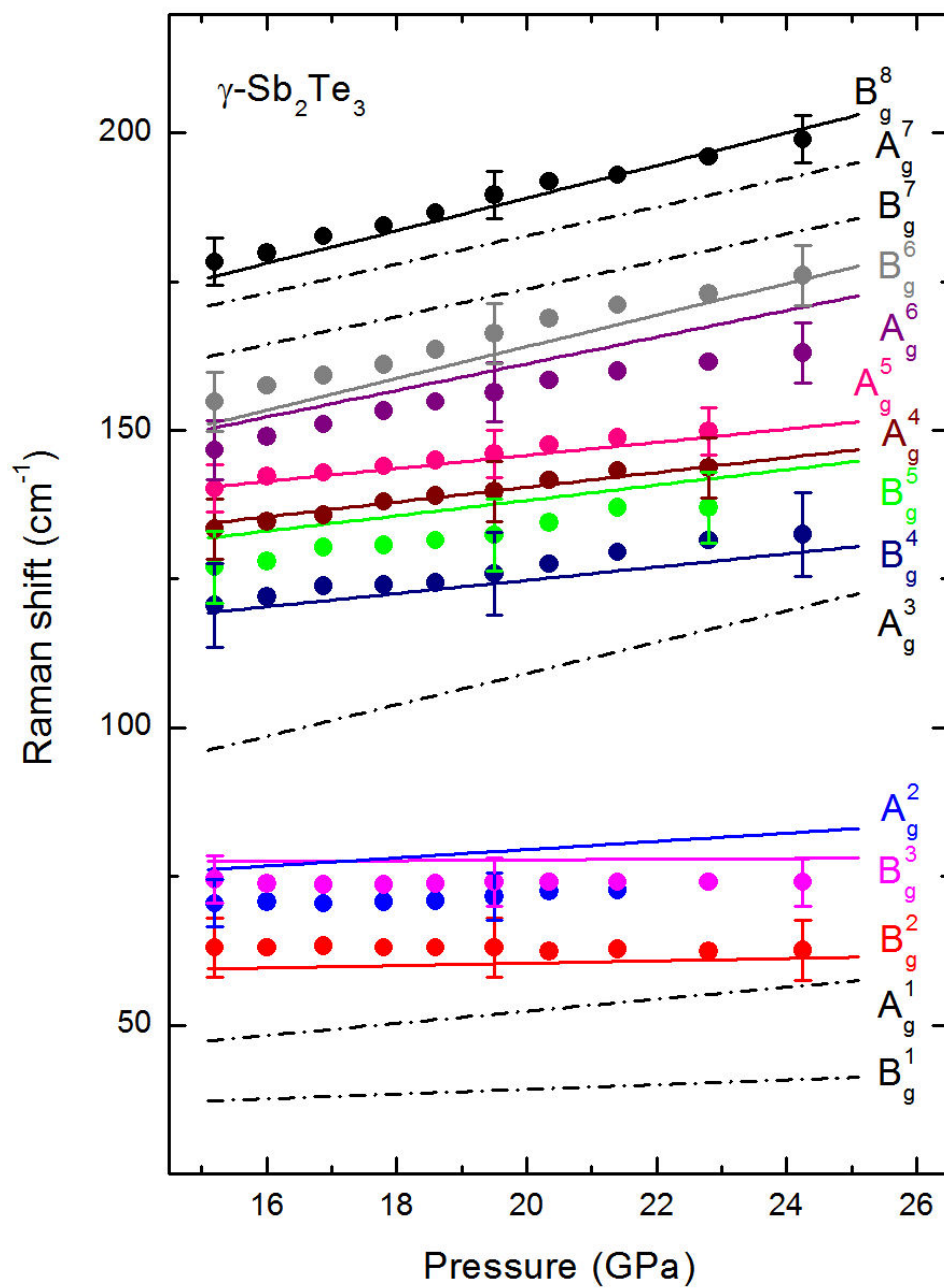


Fig. 6(a)

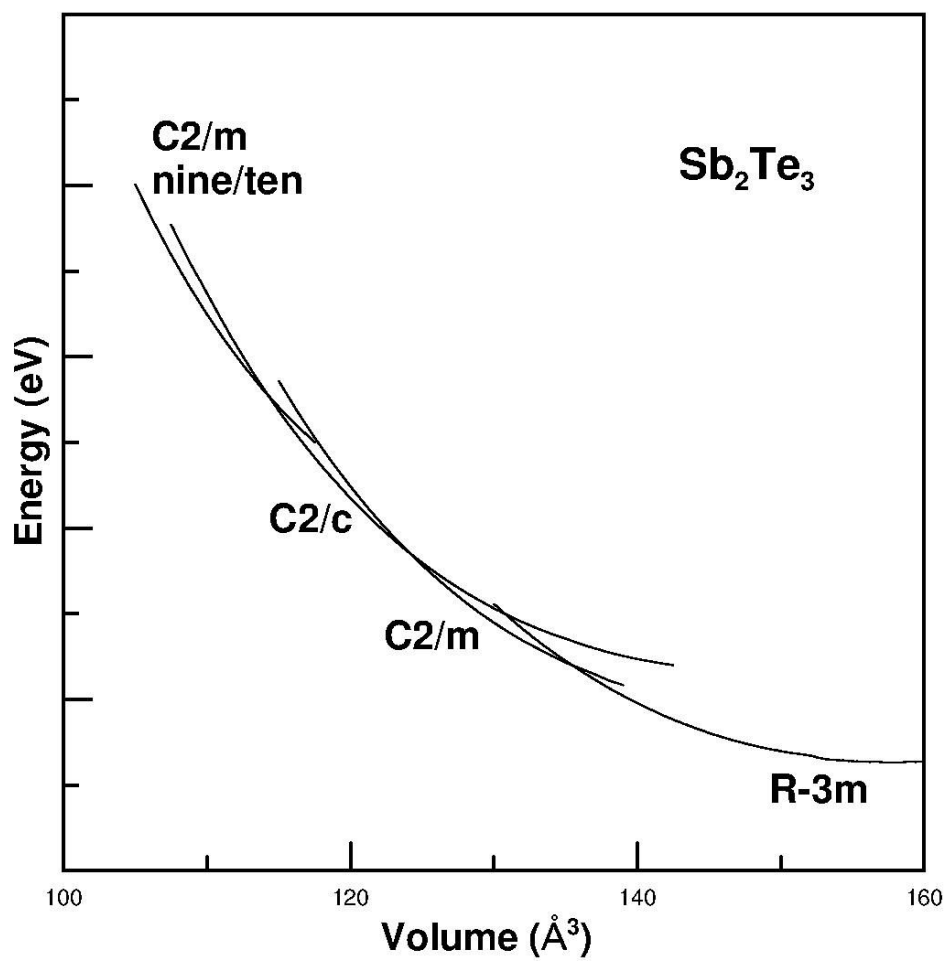
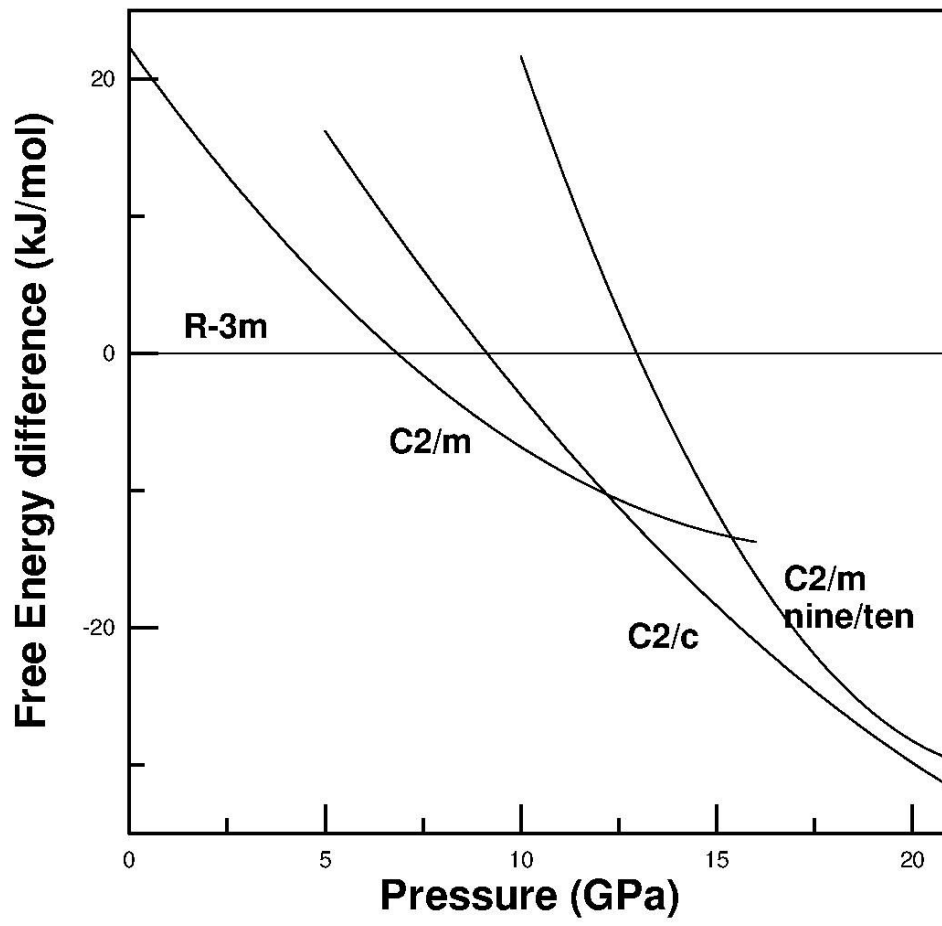


Fig. 6(b)



Lattice dynamics of Sb_2Te_3 at high pressures

O. Gomis,^{1,*} R. Vilaplana,¹ F.J. Manjón,² P. Rodríguez-Hernández,³
E. Pérez-González,³ A. Muñoz,³ V. Kucek⁴, and C. Drasar⁴

¹Centro de Tecnologías Físicas, MALTA Consolider Team, Universitat Politècnica de València, 46022 Valencia (Spain)

²Instituto de Diseño para la Fabricación y Producción Automatizada, MALTA Consolider Team, Universitat Politècnica de València, 46022 Valencia (Spain)

³MALTA Consolider Team - Departamento de Física Fundamental II, and Instituto U. de Materiales y Nanotecnología, Universidad de La Laguna, Universidad de La Laguna, 38205 La Laguna, Tenerife (Spain)

⁴Faculty of Chemical Technology, University of Pardubice, Studentská 95, 53210-Pardubice, (Czech Republic)

Correspondence and request for materials should be addressed to O. Gomis

(osgohi@fis.upv.es)

Supplementary materials

Supplementary Table I. Theoretical (th.) *ab initio* IR-mode frequencies and pressure coefficients observed in α -Sb₂Te₃ (R-3m phase) at room temperature and P₀= 1 atm, as obtained from fits to the data using $\omega(P) = \omega(P_0) + a_1 \cdot (P - P_0)$. Experimental IR-mode frequencies at room pressure are given for comparison after Ref. 41.

Mode	ω_0 (cm ⁻¹)	a_1 (cm ⁻¹ /GPa)	ω_0 (th.) (cm ⁻¹)	a_1 (th.) (cm ⁻¹ /GPa)
E _u ¹	67	-	78.0	2.95
E _u ²	-	-	100.4	1.21
A _{2u} ¹	-	-	109.9	1.91
A _{2u} ²	-	-	138.7	3.54

Supplementary Table II. Theoretical (th.) *ab initio* IR-mode frequencies and pressure coefficients observed in β -Sb₂Te₃ (C2/m phase) at room temperature at P₀= 8.6 GPa as obtained from fits using $\omega(P) = \omega(P_0) + a_1 \cdot (P - P_0)$.

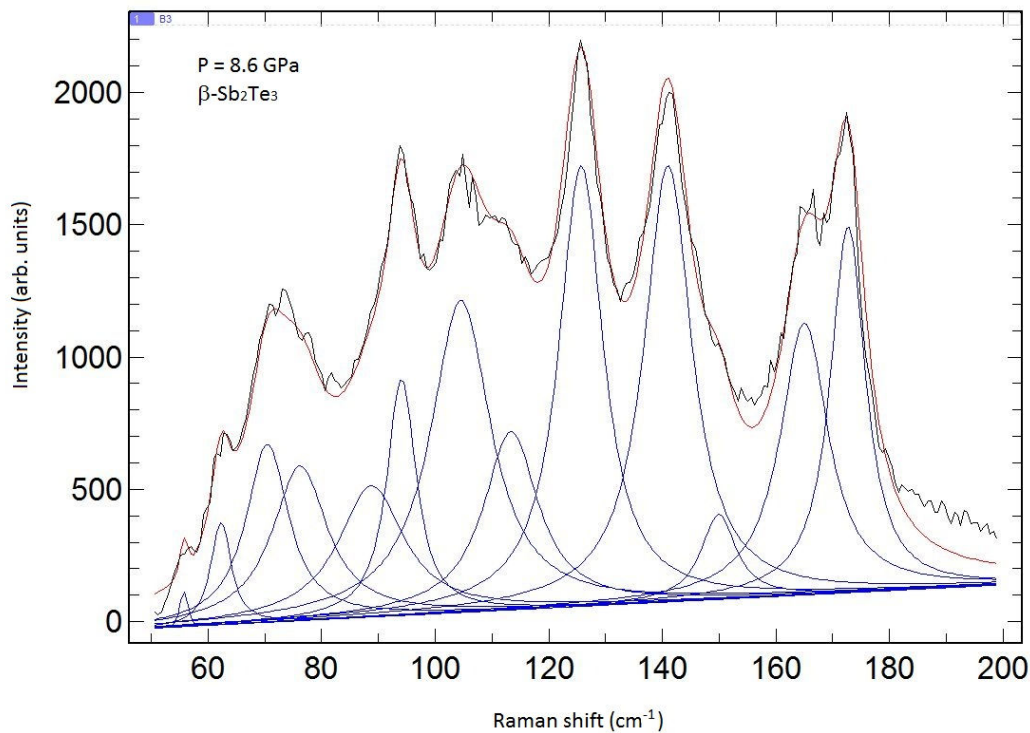
Mode	$\omega (P_0)$ (th.) (cm ⁻¹)	a_1 (th.) (cm ⁻¹ /GPa)
A _u ¹	66.9	1.92
B _u ¹	66.9	0.95
B _u ²	79.2	1.58
A _u ²	93.8	2.16
B _u ³	96.7	2.23
A _u ³	98.9	2.04
B _u ⁴	109.3	2.81
A _u ⁴	128.5	1.93
B _u ⁵	132.3	1.48
B _u ⁶	138.5	2.64
B _u ⁷	155.6	1.52
B _u ⁸	163.3	2.36

Supplementary Table III. Theoretical (th.) *ab initio* IR-mode frequencies and pressure coefficients observed in γ -Sb₂Te₃ (C2/c phase) at room temperature at P₀= 15.2 GPa as obtained from fits using $\omega(P) = \omega(P_0) + a_1 \cdot (P - P_0)$.

Mode	$\omega(P_0)$ (th.) (cm ⁻¹)	a_1 (th.) (cm ⁻¹ /GPa)
B _u ¹	53.2	0.19
A _u ¹	53.9	1.18
A _u ²	78.5	0.20
B _u ²	79.4	0.55
A _u ³	99.8	1.19
B _u ³	121.1	1.43
B _u ⁴	121.7	2.19
A _u ⁴	136.7	0.98
B _u ⁵	140.7	2.15
A _u ⁵	159.2	1.80
A _u ⁶	162.2	2.34
B _u ⁶	168.6	2.20

Supplementary Figure 1.

Raman spectrum of β -Sb₂Te₃ at 8.6 GPa decomposed into Voigt profiles. The five high-frequency peaks above 120 cm⁻¹ can be clearly attributed to Raman-active modes of the C2/m structure (see correspondence with bottom marks in Fig. 4(b) in the main text). This gives us confidence in our assignment of this phase to the C2/m structure recently found in Bi₂Te₃. The assignment of the low-frequency modes below 120 cm⁻¹ to Raman-active modes of the C2/m structure is more difficult because there are 8 Raman-active modes between 50 and 120 cm⁻¹. The two lowest-frequency Voigt lines fitted around 56 and 62 cm⁻¹ have not been attributed to Raman-active modes because they are in the region where the edge filter cuts the Raman spectrum and its pressure evolution does not seem to match to the calculated pressure dependence of the modes expected in that region. Additionally, the mode A_g² does not appear at 8.6 GPa and is detected above 10 GPa as can be seen in Figs. 4(a) and 4(b) in the main text. The rather broad band fitted at 88 cm⁻¹ cannot be assigned to β -Sb₂Te₃ and could be a second-order Raman peak. Finally, the small shoulder at about 118.4 cm⁻¹ (not fitted due to its low intensity) can be attributed to the pair A_g⁵, B_g⁵ after studying its evolution with pressure.



Supplementary Figure 2.

Raman spectrum of γ -Sb₂Te₃ at 18.6 GPa decomposed into Voigt profiles. We have attributed Raman-active modes of the C2/c structure to all Voigt peaks above 120 cm⁻¹ and below 80 cm⁻¹ (see correspondence with Fig. 5(b) in the main text). However, we have not assigned the broad band around 91 cm⁻¹ to a first-order mode because the A_g³ Raman-active mode is theoretically predicted to be around 106 cm⁻¹ at 18.6 GPa and additionally the mode at 91 cm⁻¹ is a broad band whose frequency is difficult to follow at higher pressures. Note that at least 9 bands can be clearly observed without fitting the Raman spectrum; however, the full Raman spectrum cannot be fitted with only 9 Voigt profiles.

